

# A Deeper Look into Convolutions via Pruning

Ilke Cugu<sup>a,\*</sup>, Emre Akbas<sup>a</sup>

<sup>a</sup>Department of Computer Engineering, Middle East Technical University, 06800, Ankara, Turkey

## ARTICLE INFO

### Keywords:

pruning  
model compression  
convolutional neural networks  
deep learning  
expert kernels  
eigenvalues

## ABSTRACT

Convolutional neural networks (CNNs) are able to attain better visual recognition performance than fully connected neural networks despite having much less parameters due to their parameter sharing principle. Hence, modern architectures are designed to contain a very small number of fully-connected layers, often at the end, after multiple layers of convolutions. It is interesting to observe that we can replace large fully-connected layers with relatively small groups of tiny matrices applied on the entire image. Moreover, although this strategy already reduces the number of parameters, most of the convolutions can be eliminated as well, without suffering any loss in recognition performance. However, there is no solid recipe to detect this hidden subset of convolutional neurons that is responsible for the majority of the recognition work. Hence, in this work, we use the matrix characteristics based on eigenvalues in addition to the classical weight-based importance assignment approach for pruning to shed light on the internal mechanisms of a widely used family of CNNs, namely residual neural networks (ResNets), for the image classification problem using CIFAR-10, CIFAR-100 and Tiny ImageNet datasets. The codes are available at <https://github.com/cuguilke/psykedelic>.

## 1. Introduction

Modern deep neural networks are able to attain impressive performance on computer vision problems by using millions of parameters scattered across multiple layers in the form of convolutions. However, as we show in this study, one can often eliminate most of these parameters without any negative effect on generalization error. A classical method of doing so is to prune the parameters that are effectively zero. However, in the case of pruning *groups of parameters* such as the channels in a convolutional neuron, it is not clear how to assess their importance.

In the literature, the de facto standard of assessing neuron importance is to check the average absolute value of its weights which is an acceptable proposition for fully connected neural nets [23, 22, 66, 19, 41, 64, 67, 63, 69, 7]. However, for visual recognition, convolutional neural nets (CNNs) [13, 37] have already surpassed the fully connected nets in terms of both accuracy and efficiency. CNNs reduced the number of parameters dramatically due to their parameter sharing principle and local connectivity. Although the general tendency is still to keep several fully connected (FC) layers right before the output layers [26, 64, 29], it has been shown that one can get rid off the FC layers entirely while preserving competitive performance [46, 31, 59]. Today, the modern visual recognition architectures mostly consist of convolutions. Hence, we can think of convolutions as a very effective model compression method in and of itself. However, the story does not end there since not all kernels are equally important for recognition. In the following, we refer to each  $n \times n$  channel of a convolutional neuron as a *kernel*


In fact, as we also show here, depending on the *difficulty* of a problem, it is possible that only a small portion of the

kernels are actually vital for visual recognition [39]. When the absence of a kernel results in a significant rise in the generalization error, we call that kernel an **expert kernel**, and emergence of the expert kernels are often enforced via *regularization* which is also used to limit the capacity for memorization [71]. However, several studies on the generalization properties of deep learning state that the convolutional case is more difficult to analyze [39, 3], so the theoretical advances mostly stay in the fully connected realm.

Therefore, in this work, we study convolutions and ask the question: "How can we characterize or identify expert kernels?". To this end, we focus on the fact that kernels are basically tiny matrices applied on the entire image. Thus, we employ **matrix characteristics** as heuristics to assess the significance of a given kernel. In taxonomy, this motivation puts our work under the category of **unstructured heuristic-based kernel-level pruning** of the model compression literature. Our approach is to eliminate as many kernels as possible using a set of shared hyperparameters that enable the best heuristics to maintain the recognition performance of the unpruned version of a given model without the need for a fine-tuning phase after the pruning. Then, candidate heuristics are used to provide more insight about the expert kernels in convolutional neural nets.

Discovering the correct recipe to recognize the expert kernels may influence both the theory and practice, or, at least, it may validate our current assumptions. Regarding the theory side, there are exciting empirical observations on **overparameterization** such as the lottery ticket hypothesis [12] and the double-descent in generalization error [6, 53]. These studies try to explain deep neural nets' ability to avoid overfitting despite having much more parameters than the number of available samples, and we argue that the definition of expert kernels can shed new light on the discussion on overparameterization in deep learning. In practice, elimination of non-expert kernels may produce very sparse models. As we show in this study, the sparsity structure of

\*Corresponding author

 [cuguilke@gmail.com](mailto:cuguilke@gmail.com) (I. Cugu)

ORCID(s): 0000-0002-9070-3978 (I. Cugu)

the pruned model heavily depends on the problem definition (i.e. the dataset), hence, in some cases, it is possible to remove large groups of neurons resulting in a direct drop in the computational cost. Nevertheless, such models when combined with the advances in high performance sparse matrix computations can yield families of energy efficient neural nets [60].

In this paper, we present, to the best of our knowledge, **the first extensive analysis on eigenvalue based heuristics to mark the expert kernels, the distribution of expert kernels through layers, and the change in their pruning behavior during the different phases of training.** Our findings include: (1) identification of spectral norm as a more robust heuristic (in the sense that it better preserves generalization accuracy) than the widely-used average absolute weight of a kernel, (2) feasibility of ignoring the complex parts of the eigenvalues to push the pruning ratio further without a significant loss in recognition performance, (3) dataset footprint on the active parameter distribution across layers after pruning, (4) observation of a shift in eigenvalues after the first drop in learning rate causing some heuristics to fail.

This paper is organized as follows: we start by reviewing the relevant work in the literature in Section 2. Next, we introduce our candidate heuristics to assess kernel quality in Section 3, the relevant regularization in Section 4, and our experimental setup in Section 5. Then, our analysis starts: (1) the standard performance comparison in Section 6, (2) since most of our heuristics are based on eigenvalues, we discuss real vs. complex eigenvalues in Section 7, (3) which heuristic prunes which kernels analysis in Section 8, (4) layer-wise pruning analysis in Section 9, and (5) epoch-wise pruning analysis in Section 10.

## 2. Related Works

There are several ways of model compression in deep learning such as quantization, binarization, low-rank approximation, knowledge distillation, architectural design and pruning. In this work, we are only interested in pruning since it is the only category that directly targets the **inessential** parts of deep neural nets whereas the closest family of compression techniques in this regard focuses on approximating the **overall computation** (low-rank approximation).

In the literature, some of the early examples of pruning research are done on saliency based methods [50, 38, 51, 24], and the interest continues as new deeper architectures are being introduced [49, 10, 70]. In this line of work, the importance of a unit (weight/neuron/group) is determined by its direct effect on the training error. Although the required computation is immense, and hence the emphasis is on the development of well approximators, the reasoning behind this approach is solid and straightforward.

Another line of work does pruning based on unit outputs. To our knowledge, the first study [62] of this kind look for invariants. These invariants are defined as units whose outputs do not change across different input patterns. In other words, the units that act like bias terms are removed to save

space. This is not a widely used technique anymore, perhaps it is because the large datasets of today make it hard for units to be invariant. Today, (1) the focus is on minimizing the reconstruction error of output feature maps per layer [28, 47], (2) clustering units w.r.t to their activations [11, 4, 52]. We can also count the latter studies under another category, namely clustering-based pruning [55, 65, 63, 42]. A relatively similar study [27] uses geometric median to set representative/centroid filters and prune the ones that are close to the geometric median.

Next set of studies [44, 68, 18, 72] leverage scaling factors such as the  $\gamma$  of batch norm [32] or introduce their own for different levels of analysis (neuron/group/layer) [30] to cut off the outputs of some units. The advantage of this method is that it releases the input dependency of activation based importance assignment. In other words, if the scaling factor is 0, it is guaranteed that the corresponding unit has no contribution to recognition. We can include mask based pruning methods [33, 57] under this category as well since the basic principle is the same. Although quite useful in practice, this approach does not tell us anything about the nature of a "good unit" for recognition. The decision is left entirely to the optimization by simply adding a regularization term for the scaling factors. Similarly, a recent work [43] also leaves the importance assignment to the learning itself by employing a minimax game as in generative adversarial networks [17]. One way to study this black box is to introduce heuristics and test their validity. A well-known heuristic is the average of the absolute value of the weights of a unit [23, 22, 66, 19]. Hence, we take it as a baseline for our matrix characteristics based heuristics (see Section 3).

There are also analysis papers that can be found related to ours since the motivation is the same: to understand deep convolutional neural nets via pruning. Liu et al.'s work [45] present an extensive empirical study on pruning algorithms to see if there is indeed an advantage of pruning over training the target architecture from scratch. Their methodology involves a fine-tuning phase after pruning to recover the loss in performance. In that setting, it is shown that **structured pruning** can be omitted, and, instead, one can directly train the target architecture from scratch and achieve competitive performance. However, it seems this is not the case for **unstructured pruning**. In our study, we also employ an unstructured pruning scheme, but we do not have a fine-tuning phase since our aim is to prune as much as possible while preserving the vanilla performance. On another note, pruning is argued to be important since one cannot achieve the same adversarial robustness or performance by training from scratch [69]. In addition, a recent study [7] confirms the observations of Liu et al. [45] and studies the differences between the representations of the pruned nets and vanilla nets.

## 3. Expert Kernel Heuristics

Convolutional layers are quite interesting since they can express more representational power than the fully-connected counterparts despite having much fewer parameters. How-

ever, in the pruning literature, convolutional layers are often treated as if they are fully connected layers. A common approach is to compute the average absolute weight of a given kernel (in this work, a kernel is referred to as a single channel of a neuron in a convolutional layer). However, although this technique works well in practice, it is not clear if the average weight is the real indicator of a kernel’s redundancy. Hence, we propose several heuristics that we refer to as **compression modes** throughout the paper. Our compression modes are for a given  $n \times n$  real kernel  $K$ :

- **det**: abs determinant

$$= |\det(K)|$$

If we assume values smaller than  $10^{-12}$  as effectively 0, then this mode prunes kernels that are not full-rank. Therefore, its corresponding hypothesis is that an expert kernel is a full-rank matrix.

- **det\_gram**: abs determinant of the Gramian matrix

$$= |\det(G)|$$

where  $G = K^T K$ . Since we employ weight regularization (see Section 4), kernels tend to have very small weights even if they are not pruned. Combined with a threshold value of  $10^{-24}$ , this mode checks the possible numerical instability caused by weight regularization. Formally,

$$\det(G) = \det(K^T K) = \det(K^T) \det(K) = \det(K)^2$$

which is basically the same criteria as det. However, in Section 8, we will see that the floating point constraints prevent the two compression modes from being identical.

- **min\_eig**: min abs eigenvalue

$$= \min \{ |\lambda_i(K)| \mid i \in \{1, \dots, n\} \}$$

This mode basically tests the hypothesis of det mode since the smallest absolute eigenvalue is enough to check whether a matrix is full-rank. However, det is not enough for that due to the fact that it is the product of all eigenvalues in which case the largest absolute eigenvalue may prevent an overkill.

- **min\_eig\_real**: min abs eigenvalue (real parts only)

$$= \min \{ |a_i(K)| \mid i \in \{1, \dots, n\} \}$$

where  $\lambda = a + bi$ . As explained in Section 5, we are generally dealing with  $3 \times 3$  kernels, and these matrices can have complex conjugate eigenvalues. Hence, this mode enables us to measure the relevance of the imaginary part of such eigenvalues.

- **spectral\_radius**: max abs eigenvalue

$$= \max \{ |\lambda_i(K)| \mid i \in \{1, \dots, n\} \}$$

This mode measures the largest scaling of the eigenvectors of  $K$  while being a safe comparison factor for a possible overkill due to min\_eig.

- **spectral\_radius\_real**: max abs eigenvalue (real parts only)

$$= \max \{ |a_i(K)| \mid i \in \{1, \dots, n\} \}$$

where  $\lambda = a + bi$ . It has the same reasoning with min\_eig\_real.

- **spectral\_norm**: max singular value

$$= \sqrt{\lambda_{\max}(G)}$$

where  $G = K^H K = K^T K$  since the kernel  $K$  is a real matrix. This mode is quite interesting since it is the key component of residual network invertibility [5] and stable discriminator training in GANs [48]. Hence, naturally, we also want to test the applicability of spectral norm as an importance indicator for pruning convolutional kernels. Notice that  $G$  is a  $n \times n$  real symmetric matrix, so  $\lambda_i(G) \in \mathbb{R}$  and  $\lambda_i(G) \geq 0 \forall i \in \{1, \dots, n\}$ . Thus, there is no spectral\_norm\_real mode.

- **weight**: avg of abs weights

$$= \frac{1}{n^2} \sum_i^n \sum_j^n |w_{ij}|$$

where  $w_{ij} \in K$ . This is the control group since it is the de-facto standard of pruning in practice.

Note that since the exact calculation of the eigenvalues of a matrix larger than  $4 \times 4$  is, in general, not possible, according to the insolvability theory of Abel [1] and Galois [14], some of the compression modes are only applicable to a restricted set of convolutional architectures. On the other hand, most well-known models in the literature excessively use  $3 \times 3$  kernels, and we employed a model family satisfying this constraint which is reported in Section 5.

## 4. Regularization for Pruning

Regularization in deep learning can be used for different purposes. For example, it can be used in combination with a specific activation function to limit the representational capacity of a model or it can be used just to prevent the weights from getting too large [16]. In this work, we use  $L_1$  regularization to zero out most parameters so that only a small fraction of parameters would be doing most of the recognition work. One can think of this as creating a very competitive environment where recognition resources are accumulated in a minority of kernels, and we evaluate the proposed compression modes in terms of their indication quality for such a minority.

As explained in Section 3, all compression modes apart from weight are controlled by eigenvalues.  $L_1$  regularization is a known technique to make the weights sparse [16] and, naturally, make the average absolute weight small. In this section, we will prove that it can also be used to make eigenvalues small.

Let kernel  $K$  be a  $n \times n$  real matrix,

$$K = \begin{pmatrix} w_{11} & w_{12} & \dots & w_{1n} \\ w_{21} & w_{22} & \dots & \vdots \\ \vdots & \vdots & \ddots & \vdots \\ w_{n1} & \dots & \dots & w_{nn} \end{pmatrix}$$

define radius  $r_i$  as the sum of the absolute values of the off-diagonal elements per row,

$$r_i = \sum_{j \neq i}^n |w_{ij}|$$

and let Gershgorin disk  $D_i$  be the closed disk in the complex plane centered at  $w_{ii}$  with radius  $r_i$ ,

$$D_i = \{x \in \mathbb{C} : |x - w_{ii}| \leq r_i\}$$

Then, Gershgorin Circle Theorem [15] states that every eigenvalue of the kernel  $K$  lies within at least one of the Gershgorin disks  $D_i$ .

As the weights get smaller, the origins of disks  $D_i$  move towards zero. In addition, since the off-diagonal row sums get smaller, the disks shrink. In other words, excessive  $L_1$  regularization collapses all Gershgorin disks  $D_i$  into points near zero.

In conclusion,  $L_1$  regularization minimizes (1) the average absolute weights, and (2) the probability of having large eigenvalues. We will microscope the subtle difference between the two in our analysis sections.

## 5. Experimental Setup

**Dataset.** We used 3 generic object classification datasets: {CIFAR-10 [36], CIFAR-100 [36], tiny-imagenet [40]}. CIFAR-10 and CIFAR-100 datasets are well known benchmarks for generic image classification. tiny-imagenet is a subset of ImageNet [58] originally formed as a class project benchmark, and a convenient next step after CIFAR-10 and CIFAR-100 since it provides a harder classification task (200 object classes) and we do not have enough resources to run our experiments on ImageNet. Image resolutions are  $32 \times 32$  in CIFAR, and  $64 \times 64$  in tiny-imagenet. In the analysis sections, we will show that these 3 datasets are quite useful to test the robustness of a hypothesis. We set hyperparameters using validation sets we form by randomly separating 10% of the training set where each class is represented equally. Then, we report test results in the analysis part for which we use the pre-determined test sets for CIFAR-10 and CIFAR-100 and the pre-determined validation set of tiny-imagenet (since we do not have access to the labels of its test set).

**Models.** We used a well known family of convolutional neural networks: ResNets [26]. In the original paper, ResNets come with 2 different architectures: a thin ResNet variant for CIFAR-10, and a wide ResNet variant for ImageNet. Although the latter is not specifically designed for the datasets we have, it is essential to test generalization of pruning hypotheses. Moreover, wide ResNets enables using ImageNet

pre-trained weights to test the effect of model initialization on pruning. In this study, we employ ResNets {32, 56, 110} (**thin variants**) and ResNet50 (**wide variant**).

$L_1$  **penalty.** This is the hyperparameter  $\alpha$  in Eq. 1. We tried 4 values:  $\{10^{-3}, 4 * 10^{-4}, 10^{-4}, 10^{-5}\}$ . Naturally, among these,  $10^{-3}$  results in the highest pruning rate and the lowest validation accuracy.  $10^{-5}$  produced slightly better classification performance than  $10^{-4}$ , but with a significantly lower pruning rate.  $4 * 10^{-4}$  was able to reach as high as  $\approx 96\%$  pruning rate (for example using ResNet110 for CIFAR-10 with weight or spectral radius as the compression mode while preserving a reasonable validation accuracy of  $\approx 81\%$ ) resulting in very sparse models. However, when we set performance of training without weight regularization as baseline, the gap between the validation accuracy of  $4 * 10^{-4}$  and the baseline grows as the dataset gets more complex (CIFAR-10  $\rightarrow$  CIFAR-100  $\rightarrow$  tiny-imagenet). Therefore, in our analyses  $L_1$  penalty  $\alpha = 10^{-4}$ .

$$L_1 \text{ loss term} = \alpha \sum_{i=0}^n |w_i| \tag{1}$$

**Significance threshold.** In Section 3, we explain how each compression mode computes the significance score of a kernel. Instead of targeting kernels which have significance score of exactly 0, we define a threshold and deem the kernels that have scores under this threshold as insignificant. Hence we name this hyperparameter as significance threshold. In Fig 1 and 2, we show the pruning ratio of each compression mode for different significance thresholds to make an informed decision on how to define what values we will take as effectively zero. In Fig 1, we see similar curves for thin ResNets, and, as expected, the pruning ratio increases as we go from ResNet32 to ResNet110. Moreover, since det and det\_gram modes represent multiplication of eigenvalues/matrices, their curves go significantly above others, so it is important to scale their selected threshold accordingly.

Another interesting finding is that CIFAR-100 task results in the least pruning ratio compared to CIFAR-10 and tiny-imagenet. We will analyze the effect of this phenomenon on recognition performance in Section 6. In Fig 2, the model at hand is ResNet50, which is wider than the ones mentioned before, so it has a different curve. With ResNet50, our goal is to examine the effect of initial weights on pruning. Surprisingly, the pruning ratio curve is similar under different initializations, and it is important to notice that imagenet\_init is substantially different than others since it can actually be used to correctly classify most objects in ImageNet. In addition, in both Figs 1 and 2, we see compression modes except det and det\_gram draw quite similar curves where green-ish ones (min\_eig based) go above red-ish ones. This is the expected behavior of extremums and it is discussed in detail in Sections 6 and 8. As we want to prune the models as much as possible, we did preliminary experiments on a small targeted interval of significance thresholds ( $10^{-5} \rightarrow 10^{-3}$ ). We found  $10^{-4}$  to have a good balance between accuracy and pruning ratio.

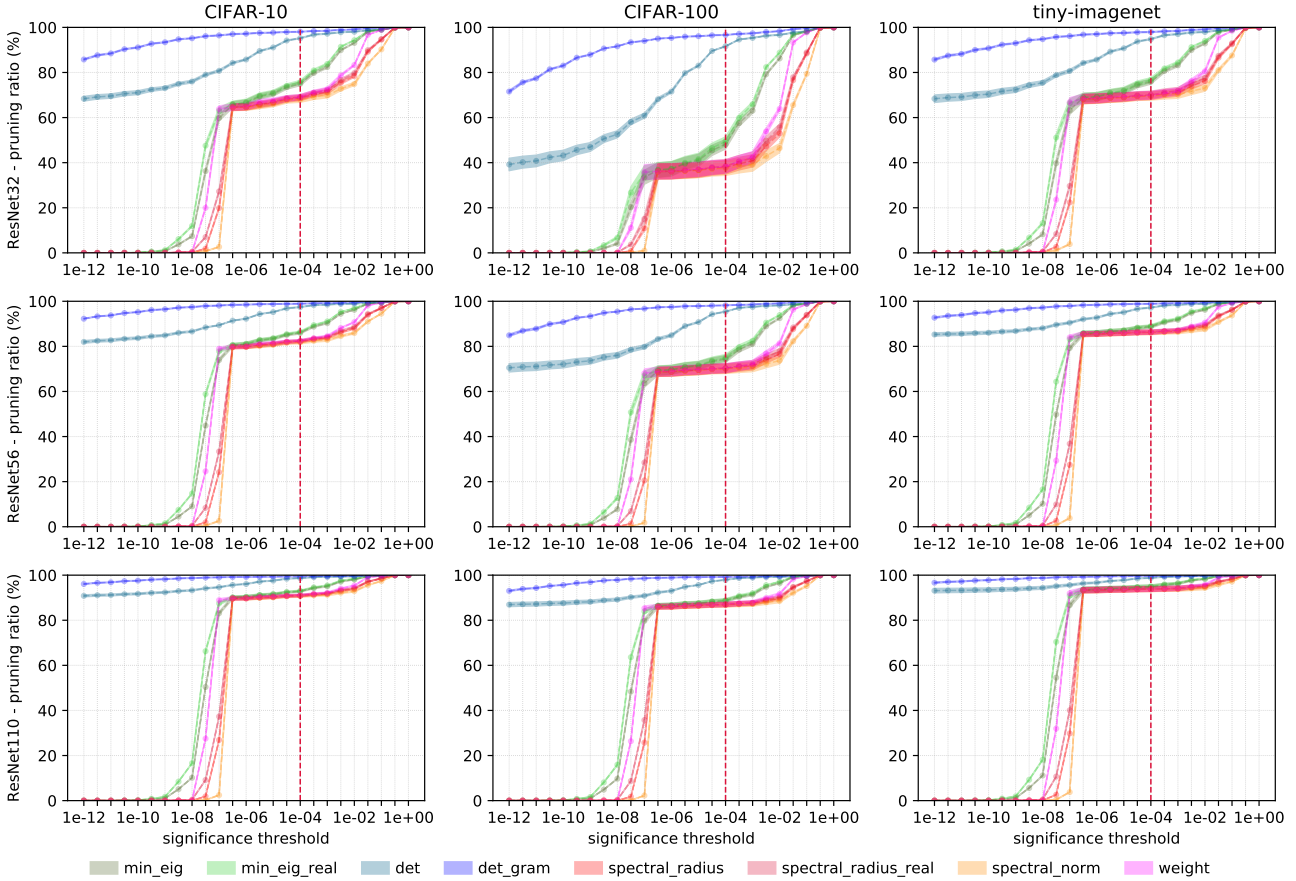


Figure 1: Pruning ratio vs. threshold chart for thin ResNets under multiple random initializations.

In conclusion, in our analysis, we set the significance threshold as:

- det:  $10^{-12}$  for 3x3 kernels,  $10^{-4}$  for 1x1 kernels
- det\_gram:  $10^{-24}$  for 3x3 kernels,  $10^{-8}$  for 1x1 kernels
- others:  $10^{-4}$

**Statistical significance.** We repeated each run for 15+ times, and for performance comparison this number goes up to 40+ times simply due to the chronological order of the implementations. Note that each run implies a particular combination of the settings:  $f_{\text{settings}}$  (model, dataset, initialization mode). For different comparison modes, the training part is shared. Once the training stops, all compression modes branch off. Hence, the experimental results do not have a random parameter space noise for different compression modes.

**Other hyperparameters.** We wanted to keep all hyperparameters constant as much as possible to rule out unwanted noise due to variance of hyperparameters for controlled experiments, so unless specifically indicated, a given value for a hyperparameter holds for all settings (models, datasets, etc.):

- Optimization algorithm. In this study, we used Adam optimizer [35] due to its fast convergence on the datasets we use.

- Learning rate. For ResNets {32, 56, 110}, the base learning rate is  $10^{-3}$  whereas it is  $10^{-4}$  for ResNet50, and for both families it is divided by 10 at epochs 80, 120 and 160.
- Batch size. We tried 32, 64, and 128, but we did not find a significant or constant advantage for a particular selection. Therefore, in order to speed-up the experiments, we selected 128 as the mini batch size.
- Epochs. We monitored the validation accuracy of all models for all datasets, and decided to stop the training at a safe point (validation accuracy curve becomes flat). Hence, the number of epochs is 200, which is an extremely safe point for some cases where learning stabilizes very early on. In Section 10, we examine the pruning through epochs and try to shed some light onto the internal structure of CNNs during training.
- Initialization. We have 3 initialization modes:
  - random\_init: Models are initialized using He normal initialization [25] option in Keras [8].
  - static\_init: We still use He initialization, but we import the same frozen initial weight for each run (we run the experiments multiple times to check statistical significance of the results). This

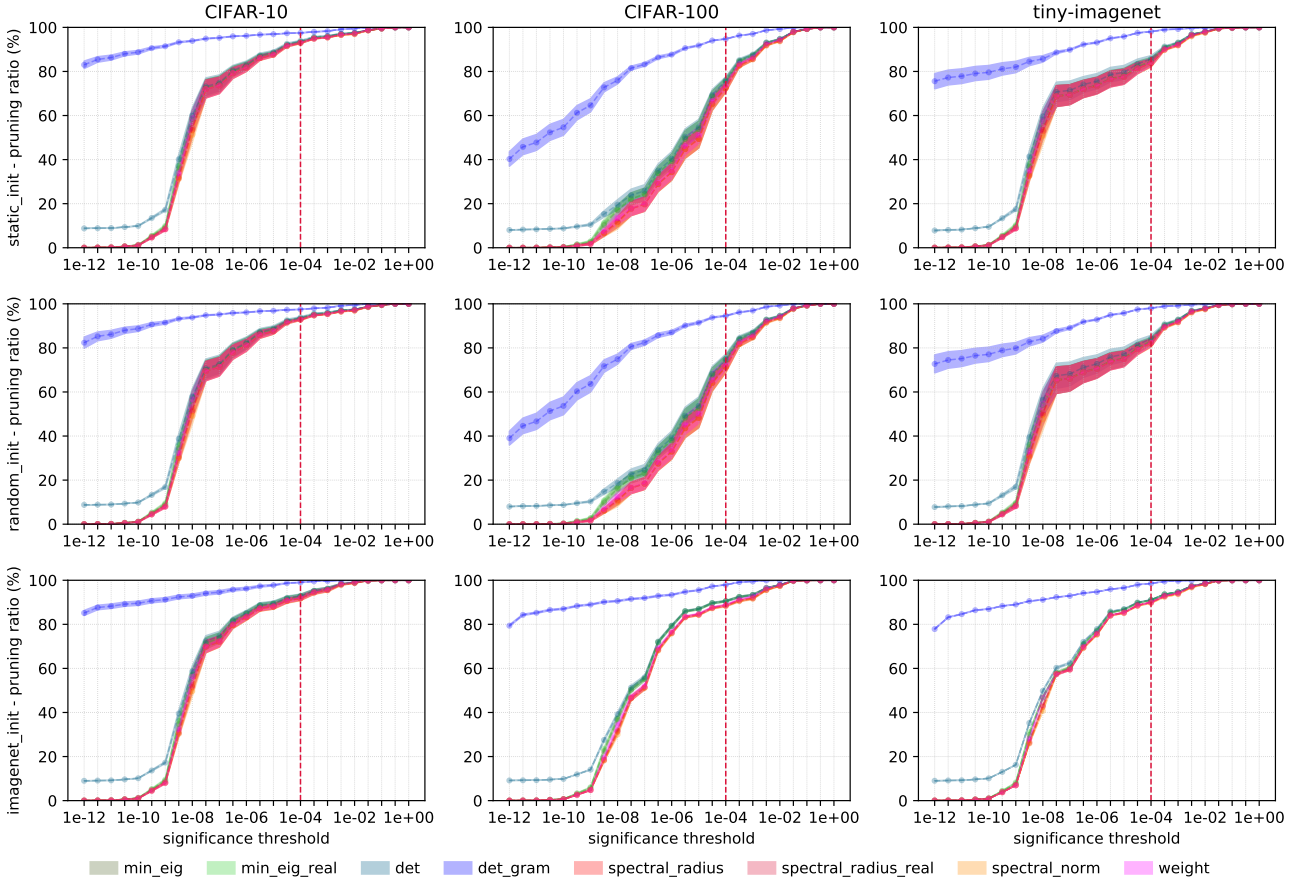


Figure 2: Pruning ratio vs. threshold chart for ResNet50 under different initializations.

mode provides a control group for random\_init experiments since we do not have a variance in initial conditions here.

- imagenet\_init: This mode is only available for ResNet50 experiments. Nevertheless, since our compression modes are tightly coupled with the properties of the convolution matrices in models, it is important to test the robustness of our propositions in an unfamiliar parameter space where initial conditions are not random.

## 6. Performance Comparison

Summary of findings:

- Any heuristic that uses the min abs eigenvalue is bad.
- Expert kernel  $\neq$  full-rank matrix.
- Spectral norm is the strongest candidate since it causes almost no drop in classification accuracy.
- Spectral radius and the avg abs weight are the leading heuristics in terms of compression score (Table 4).

In this section, we compare the compression modes in terms of classification accuracy and pruning ratio which is the number of pruned kernels divided by the total number of

kernels. These two majors are inversely correlated. Hence, to provide a relatively unified view of compression performance we include an additional major called **compression score**  $c$  defined as,

$$c = \frac{acc_{pruned}}{acc_{vanilla}} * \frac{\# \text{ of pruned weights}}{\text{total} \# \text{ of weights}}$$

Notice that,  $c$  may be larger than 1 if pruning removes disruptive kernels that are causing misclassifications. However, in our experiments, we did not encounter such a scenario. Nevertheless, higher the  $c$  the better.

At the end of a training, we first evaluate the classification accuracy without pruning ( $acc_{vanilla}$ ), then each compression mode branches-off from that same parameter state to evaluate their performance. In other words, trained weights are the same for all modes, but the set of pruned kernels changes.

If you trim a neural net and do not receive a severe penalty for it, it is a good indicator that the thrown-out parts were not necessary in the first place. However, we do not search for a set of desirable hyperparameters for each compression mode to get  $\frac{acc_{pruned}}{acc_{vanilla}} \approx 1$ . Instead, we set the environment where at least one compression mode is able to prune the network while achieving competitive performance to the vanilla network (see "None" category in Table 1).

**Table 1**  
Classification accuracy comparison of different compression modes

	compression mode	ResNet32		ResNet56		ResNet110		ResNet50		
		static	random	static	random	static	random	static	random	imagenet
CIFAR-10	None	0.8935 ± 0.002	0.8920 ± 0.003	0.8921 ± 0.002	0.8919 ± 0.002	0.8908 ± 0.003	0.8858 ± 0.005	0.7652 ± 0.003	0.7632 ± 0.004	0.8693 ± 0.002
	min_eig	0.6622 ± 0.075	0.6548 ± 0.095	0.6503 ± 0.088	0.6384 ± 0.109	0.6713 ± 0.074	0.6510 ± 0.105	0.1808 ± 0.052	0.2370 ± 0.049	0.1375 ± 0.021
	min_eig_real	0.6283 ± 0.081	0.6342 ± 0.106	0.6277 ± 0.090	0.5991 ± 0.101	0.6381 ± 0.085	0.6263 ± 0.112	0.1759 ± 0.051	0.2330 ± 0.051	0.1353 ± 0.020
	det	0.8932 ± 0.002	0.8910 ± 0.003	0.8913 ± 0.002	0.8910 ± 0.002	0.8906 ± 0.003	0.8854 ± 0.005	0.6617 ± 0.059	0.6874 ± 0.022	0.5696 ± 0.043
	det_gram	0.8931 ± 0.002	0.8915 ± 0.002	0.8916 ± 0.002	0.8915 ± 0.002	<b>0.8908</b> ± 0.003	0.8854 ± 0.005	0.6625 ± 0.059	0.6878 ± 0.022	0.5713 ± 0.042
	spectral_radius	<b>0.8935</b> ± 0.002	<b>0.8920</b> ± 0.003	<b>0.8921</b> ± 0.002	0.8918 ± 0.002	0.8907 ± 0.003	<b>0.8858</b> ± 0.005	<b>0.7634</b> ± 0.006	<b>0.7612</b> ± 0.007	0.8689 ± 0.003
	spectral_radius_real	0.8921 ± 0.002	0.8910 ± 0.003	0.8907 ± 0.002	0.8908 ± 0.003	0.8899 ± 0.003	0.8846 ± 0.004	<b>0.7634</b> ± 0.005	0.7606 ± 0.006	0.8679 ± 0.002
	spectral_norm	<b>0.8935</b> ± 0.002	<b>0.8920</b> ± 0.003	<b>0.8921</b> ± 0.002	<b>0.8919</b> ± 0.002	<b>0.8908</b> ± 0.003	<b>0.8858</b> ± 0.005	0.7631 ± 0.007	0.7611 ± 0.007	<b>0.8692</b> ± 0.003
	weight	<b>0.8935</b> ± 0.002	<b>0.8920</b> ± 0.003	<b>0.8921</b> ± 0.002	0.8918 ± 0.002	0.8907 ± 0.003	<b>0.8858</b> ± 0.005	0.7619 ± 0.007	0.7605 ± 0.006	<b>0.8692</b> ± 0.003
CIFAR-100	None	0.6487 ± 0.004	0.6467 ± 0.005	0.6377 ± 0.005	0.6389 ± 0.004	0.6185 ± 0.010	0.6148 ± 0.009	0.4496 ± 0.005	0.4470 ± 0.005	0.5997 ± 0.003
	min_eig	0.4265 ± 0.039	0.3859 ± 0.056	0.4202 ± 0.044	0.4284 ± 0.041	0.4597 ± 0.052	0.4605 ± 0.035	0.0130 ± 0.003	0.0131 ± 0.004	0.0126 ± 0.002
	min_eig_real	0.4025 ± 0.036	0.3602 ± 0.059	0.3960 ± 0.050	0.4071 ± 0.037	0.4419 ± 0.045	0.4367 ± 0.032	0.0128 ± 0.003	0.0130 ± 0.004	0.0127 ± 0.002
	det	0.6482 ± 0.004	0.6462 ± 0.005	0.6362 ± 0.006	0.6382 ± 0.004	0.6180 ± 0.010	0.6146 ± 0.009	0.1632 ± 0.054	0.1756 ± 0.038	0.0929 ± 0.013
	det_gram	0.6483 ± 0.004	0.6464 ± 0.005	0.6366 ± 0.005	0.6386 ± 0.004	0.6179 ± 0.010	0.6147 ± 0.009	0.1644 ± 0.054	0.1778 ± 0.038	0.0943 ± 0.013
	spectral_radius	<b>0.6487</b> ± 0.004	<b>0.6467</b> ± 0.005	<b>0.6377</b> ± 0.005	0.6388 ± 0.004	0.6184 ± 0.010	<b>0.6148</b> ± 0.009	0.4389 ± 0.006	0.4381 ± 0.004	0.5932 ± 0.004
	spectral_radius_real	0.6474 ± 0.004	0.6451 ± 0.005	0.6368 ± 0.006	0.6381 ± 0.004	0.6179 ± 0.010	0.6144 ± 0.009	0.4383 ± 0.005	0.4375 ± 0.004	0.5856 ± 0.004
	spectral_norm	<b>0.6487</b> ± 0.004	<b>0.6467</b> ± 0.005	<b>0.6377</b> ± 0.005	<b>0.6389</b> ± 0.004	<b>0.6185</b> ± 0.010	0.6147 ± 0.009	<b>0.4395</b> ± 0.006	<b>0.4386</b> ± 0.004	<b>0.5997</b> ± 0.003
	weight	<b>0.6487</b> ± 0.004	0.6466 ± 0.005	<b>0.6377</b> ± 0.005	0.6388 ± 0.004	0.6184 ± 0.010	0.6147 ± 0.009	0.4019 ± 0.024	0.3940 ± 0.041	0.5990 ± 0.004
tiny-imagenet	None	0.4662 ± 0.004	0.4645 ± 0.006	0.4555 ± 0.006	0.4543 ± 0.005	0.4375 ± 0.009	0.4380 ± 0.011	0.4248 ± 0.011	0.4201 ± 0.013	0.5441 ± 0.004
	min_eig	0.1440 ± 0.036	0.1262 ± 0.040	0.1554 ± 0.032	0.1380 ± 0.046	0.1781 ± 0.044	0.1720 ± 0.043	0.2659 ± 0.019	0.2814 ± 0.025	0.1345 ± 0.011
	min_eig_real	0.1242 ± 0.037	0.1073 ± 0.041	0.1489 ± 0.035	0.1290 ± 0.042	0.1587 ± 0.044	0.1585 ± 0.047	0.2378 ± 0.021	0.2567 ± 0.027	0.1125 ± 0.014
	det	0.4651 ± 0.004	0.4637 ± 0.005	0.4553 ± 0.006	0.4526 ± 0.005	0.4367 ± 0.009	0.4378 ± 0.011	0.4208 ± 0.013	0.4166 ± 0.013	0.4582 ± 0.006
	det_gram	0.4655 ± 0.004	0.4639 ± 0.006	<b>0.4556</b> ± 0.006	0.4533 ± 0.005	0.4370 ± 0.009	0.4374 ± 0.011	0.4205 ± 0.013	0.4160 ± 0.012	0.4665 ± 0.005
	spectral_radius	<b>0.4662</b> ± 0.004	0.4644 ± 0.006	<b>0.4556</b> ± 0.006	<b>0.4542</b> ± 0.005	<b>0.4376</b> ± 0.009	0.4380 ± 0.011	0.4224 ± 0.011	<b>0.4186</b> ± 0.013	0.5393 ± 0.003
	spectral_radius_real	0.4615 ± 0.005	0.4622 ± 0.005	0.4519 ± 0.008	0.4478 ± 0.009	0.4354 ± 0.009	0.4367 ± 0.011	0.4223 ± 0.012	0.4174 ± 0.013	0.5277 ± 0.003
	spectral_norm	0.4661 ± 0.004	<b>0.4645</b> ± 0.006	0.4555 ± 0.006	<b>0.4542</b> ± 0.005	0.4375 ± 0.009	<b>0.4381</b> ± 0.011	<b>0.4228</b> ± 0.011	0.4185 ± 0.013	<b>0.5442</b> ± 0.004
	weight	<b>0.4662</b> ± 0.004	0.4644 ± 0.006	<b>0.4556</b> ± 0.006	<b>0.4542</b> ± 0.005	0.4375 ± 0.009	<b>0.4381</b> ± 0.011	0.4225 ± 0.011	<b>0.4186</b> ± 0.013	0.5441 ± 0.004

In Table 1, we see very similar performance measurements for modes based on spectral radius, spectral norm and the average absolute weight. The worst results obtained by the modes that check the minimum absolute eigenvalue. Since the determinant combines both the negative and the positive results through multiplication of eigenvalues, det and det\_gram modes oscillate between the extremums. **This finding rules out the hypothesis that an expert kernel must be a full-rank matrix under the assumption that a value smaller than the selected significance threshold is effectively 0.** Because, if the minimum absolute eigenvalue is 0, the determinant is 0. However, since the values are not **exactly** 0, spectral radius often protects determinant from an overkill. We can clearly see the case where this is not enough in ResNet50 results where the gap between the extremums is large enough to significantly deteriorate the performance of determinant based modes. In Table 2, naturally, we observe the opposite, and in Table 3 we get the combined effect of both view points. For ResNets{32, 56, 110}, determinant based heuristics achieve competitive pruning performance. However, when we examine the ResNet50 case (especially the imagenet\_init results), it is clear that any compression mode taking the minimum absolute eigenvalue into account is quite unstable. Therefore, we have a compelling case to turn our attention to **spectral radius, spectral norm and the average absolute weight.**

As a side note, according to the experimental results, ignoring the complex parts of the eigenvalues results in different behavior for min\_eig and spectral\_radius modes, which will be discussed in detail in Section 7. Moreover, we see differences between the results of det and det\_gram modes. This indicates that there is indeed a relatively small numerical instability regarding the matrix operations in the given

parameter space, and this will be confirmed in Section 8 in detail.

## 7. Real vs. Complex Eigenvalues

Summary of findings:

- spectral\_radius and spectral\_radius\_real has no major difference in terms of their pruning statistics. Hence, it seems that the real part (scaling factor) of the largest absolute eigenvalue is the key part of the spectral\_radius as a kernel importance assignment heuristic.
- Since min\_eig has already started to prune essential kernels, min\_eig\_real makes the performance even worse by pruning even more essential kernels.

Here, we are interested in using eigenvalues to understand inner mechanisms of deep convolutional neural nets. One of the reasons is the geometric meaning of eigenvalues: real parts indicate **scaling** whereas complex parts indicate **rotation**. Hence, one might **conjecture**: the amount of scaling is the key indicator of an expert kernel. It is not easy to answer this question empirically since the absence of a possible drop in performance, when we ignore the complex parts, does not guarantee a general rule. On the other hand, if we actually observe a performance loss, we can rule out this hypothesis. Therefore, we have min\_eig\_real and spectral\_radius\_real modes in addition to the vanilla ones: min\_eig and spectral\_radius.

The real-part-only modes are expected to prune more kernels than their vanilla counterparts since:

$$\sqrt{a^2 + b^2} \geq a$$

**Table 2**  
Compression ratio comparison of different compression modes

compression mode		ResNet32		ResNet56		ResNet110		ResNet50		
		static	random	static	random	static	random	static	random	imagenet
CIFAR-10	min_eig	0.7454 ± 0.004	0.7536 ± 0.008	0.8567 ± 0.003	0.8581 ± 0.004	0.9217 ± 0.002	0.9225 ± 0.003	0.9306 ± 0.001	0.9303 ± 0.002	0.9401 ± 0.006
	min_eig_real	<b>0.7535</b> ± 0.003	<b>0.7611</b> ± 0.007	<b>0.8612</b> ± 0.003	<b>0.8626</b> ± 0.004	<b>0.9239</b> ± 0.002	<b>0.9247</b> ± 0.003	<b>0.9312</b> ± 0.001	<b>0.9309</b> ± 0.002	<b>0.9412</b> ± 0.006
	det	0.6969 ± 0.005	0.7063 ± 0.010	0.8290 ± 0.004	0.8302 ± 0.006	0.9084 ± 0.003	0.9087 ± 0.004	0.9262 ± 0.001	0.9257 ± 0.002	0.9322 ± 0.006
	det_gram	0.6967 ± 0.005	0.7062 ± 0.010	0.8290 ± 0.004	0.8301 ± 0.006	0.9084 ± 0.003	0.9086 ± 0.004	0.9262 ± 0.001	0.9257 ± 0.002	0.9321 ± 0.006
	spectral_radius	0.6788 ± 0.006	0.6883 ± 0.012	0.8182 ± 0.005	0.8196 ± 0.006	0.9031 ± 0.003	0.9033 ± 0.005	0.9096 ± 0.004	0.9077 ± 0.004	0.8953 ± 0.010
	spectral_radius_real	0.6830 ± 0.006	0.6924 ± 0.011	0.8208 ± 0.005	0.8220 ± 0.006	0.9043 ± 0.003	0.9045 ± 0.005	0.9106 ± 0.004	0.9087 ± 0.004	0.8972 ± 0.010
	spectral_norm	0.6722 ± 0.006	0.6816 ± 0.012	0.8141 ± 0.005	0.8159 ± 0.007	0.9012 ± 0.003	0.9015 ± 0.005	0.9072 ± 0.004	0.9050 ± 0.004	0.8890 ± 0.010
	weight	0.6832 ± 0.006	0.6924 ± 0.011	0.8209 ± 0.004	0.8222 ± 0.006	0.9045 ± 0.003	0.9048 ± 0.005	0.9168 ± 0.003	0.9152 ± 0.003	0.9091 ± 0.008
	CIFAR-100	min_eig	0.4489 ± 0.011	0.4853 ± 0.021	0.7466 ± 0.007	0.7437 ± 0.014	0.8796 ± 0.010	0.8801 ± 0.007	0.8150 ± 0.009	0.8076 ± 0.013
min_eig_real		<b>0.4641</b> ± 0.011	<b>0.4987</b> ± 0.020	<b>0.7525</b> ± 0.006	<b>0.7494</b> ± 0.014	<b>0.8820</b> ± 0.009	<b>0.8823</b> ± 0.006	<b>0.8164</b> ± 0.009	<b>0.8091</b> ± 0.013	<b>0.9275</b> ± 0.002
det		0.3518 ± 0.014	0.3993 ± 0.028	0.7109 ± 0.009	0.7084 ± 0.018	0.8657 ± 0.012	0.8666 ± 0.009	0.7825 ± 0.009	0.7736 ± 0.013	0.9195 ± 0.002
det_gram		0.3515 ± 0.014	0.3990 ± 0.028	0.7107 ± 0.009	0.7083 ± 0.018	0.8656 ± 0.013	0.8665 ± 0.009	0.7824 ± 0.009	0.7735 ± 0.013	0.9194 ± 0.002
spectral_radius		0.3301 ± 0.016	0.3812 ± 0.030	0.7029 ± 0.010	0.7011 ± 0.019	0.8619 ± 0.013	0.8629 ± 0.009	0.6750 ± 0.022	0.6625 ± 0.026	0.8255 ± 0.004
spectral_radius_real		0.3360 ± 0.015	0.3861 ± 0.030	0.7051 ± 0.010	0.7031 ± 0.019	0.8628 ± 0.013	0.8637 ± 0.009	0.6778 ± 0.022	0.6653 ± 0.026	0.8272 ± 0.004
spectral_norm		0.3244 ± 0.016	0.3764 ± 0.032	0.7005 ± 0.010	0.6989 ± 0.019	0.8607 ± 0.013	0.8616 ± 0.009	0.6703 ± 0.022	0.6576 ± 0.026	0.8138 ± 0.004
weight		0.3346 ± 0.015	0.3848 ± 0.030	0.7045 ± 0.010	0.7026 ± 0.019	0.8628 ± 0.013	0.8637 ± 0.009	0.7319 ± 0.012	0.7203 ± 0.017	0.8392 ± 0.004
tiny-imagenet		min_eig	0.6883 ± 0.005	0.6873 ± 0.010	0.8335 ± 0.006	0.8357 ± 0.005	0.9163 ± 0.004	0.9142 ± 0.007	0.8430 ± 0.013	0.8319 ± 0.011
	min_eig_real	<b>0.6946</b> ± 0.005	<b>0.6943</b> ± 0.010	<b>0.8363</b> ± 0.006	<b>0.8385</b> ± 0.004	<b>0.9174</b> ± 0.004	<b>0.9155</b> ± 0.006	<b>0.8495</b> ± 0.011	<b>0.8390</b> ± 0.010	<b>0.9200</b> ± 0.000
	det	0.6422 ± 0.008	0.6377 ± 0.015	0.8135 ± 0.008	0.8156 ± 0.007	0.9087 ± 0.005	0.9055 ± 0.009	0.8172 ± 0.017	0.8056 ± 0.016	0.9076 ± 0.000
	det_gram	0.6420 ± 0.008	0.6376 ± 0.015	0.8135 ± 0.008	0.8155 ± 0.007	0.9087 ± 0.005	0.9055 ± 0.009	0.8172 ± 0.017	0.8056 ± 0.016	0.9074 ± 0.000
	spectral_radius	0.6352 ± 0.008	0.6295 ± 0.016	0.8102 ± 0.008	0.8122 ± 0.007	0.9073 ± 0.005	0.9040 ± 0.010	0.8030 ± 0.021	0.7900 ± 0.021	0.8671 ± 0.000
	spectral_radius_real	0.6381 ± 0.008	0.6328 ± 0.016	0.8115 ± 0.008	0.8134 ± 0.007	0.9077 ± 0.005	0.9045 ± 0.009	0.8064 ± 0.020	0.7937 ± 0.020	0.8698 ± 0.000
	spectral_norm	0.6336 ± 0.008	0.6276 ± 0.016	0.8094 ± 0.008	0.8113 ± 0.008	0.9068 ± 0.005	0.9035 ± 0.010	0.7988 ± 0.022	0.7854 ± 0.023	0.8497 ± 0.001
	weight	0.6364 ± 0.008	0.6310 ± 0.016	0.8109 ± 0.008	0.8128 ± 0.007	0.9076 ± 0.005	0.9043 ± 0.010	0.8128 ± 0.015	0.8012 ± 0.015	0.8678 ± 0.000

**Table 3**  
Compression score  $c$  comparison of different compression modes

compression mode		ResNet32		ResNet56		ResNet110		ResNet50		
		static	random	static	random	static	random	static	random	imagenet
CIFAR-10	min_eig	0.5524 ± 0.062	0.5533 ± 0.081	0.6244 ± 0.084	0.6143 ± 0.105	0.6948 ± 0.078	0.6782 ± 0.110	0.2198 ± 0.063	0.2889 ± 0.060	0.1487 ± 0.023
	min_eig_real	0.5298 ± 0.068	0.5411 ± 0.091	0.6059 ± 0.087	0.5796 ± 0.098	0.6621 ± 0.089	0.6542 ± 0.118	0.2140 ± 0.062	0.2842 ± 0.062	0.1465 ± 0.021
	det	<b>0.6966</b> ± 0.005	0.7056 ± 0.010	0.8283 ± 0.004	0.8293 ± 0.005	0.9083 ± 0.003	<b>0.9083</b> ± 0.004	0.8011 ± 0.072	0.8339 ± 0.028	0.6106 ± 0.045
	det_gram	0.6964 ± 0.005	<b>0.7058</b> ± 0.010	<b>0.8285</b> ± 0.004	<b>0.8297</b> ± 0.005	<b>0.9084</b> ± 0.003	0.9083 ± 0.004	0.8021 ± 0.072	0.8343 ± 0.028	0.6124 ± 0.043
	spectral_radius	0.6788 ± 0.006	0.6883 ± 0.012	0.8182 ± 0.005	0.8196 ± 0.006	0.9031 ± 0.003	0.9034 ± 0.005	0.9075 ± 0.006	0.9054 ± 0.008	0.8948 ± 0.010
	spectral_radius_real	0.6819 ± 0.006	0.6916 ± 0.011	0.8195 ± 0.005	0.8210 ± 0.006	0.9035 ± 0.003	0.9033 ± 0.005	0.9085 ± 0.006	0.9057 ± 0.007	0.8957 ± 0.010
	spectral_norm	0.6722 ± 0.006	0.6816 ± 0.012	0.8141 ± 0.005	0.8159 ± 0.007	0.9012 ± 0.003	0.9015 ± 0.005	0.9047 ± 0.008	0.9025 ± 0.008	0.8889 ± 0.010
	weight	0.6832 ± 0.006	0.6924 ± 0.011	0.8209 ± 0.004	0.8222 ± 0.006	0.9045 ± 0.003	0.9048 ± 0.005	<b>0.9129</b> ± 0.007	<b>0.9120</b> ± 0.008	<b>0.9091</b> ± 0.009
	CIFAR-100	min_eig	0.2954 ± 0.030	0.2904 ± 0.050	0.4922 ± 0.053	0.4985 ± 0.045	0.6550 ± 0.083	0.6596 ± 0.053	0.0235 ± 0.005	0.0236 ± 0.006
min_eig_real		0.2881 ± 0.028	0.2785 ± 0.052	0.4676 ± 0.061	0.4774 ± 0.042	0.6311 ± 0.072	0.6271 ± 0.050	0.0233 ± 0.005	0.0235 ± 0.006	0.0196 ± 0.004
det		<b>0.3516</b> ± 0.014	<b>0.3990</b> ± 0.027	0.7092 ± 0.009	0.7076 ± 0.019	<b>0.8650</b> ± 0.013	0.8663 ± 0.009	0.2837 ± 0.092	0.3044 ± 0.068	0.1425 ± 0.020
det_gram		0.3513 ± 0.014	0.3988 ± 0.027	<b>0.7096</b> ± 0.010	<b>0.7080</b> ± 0.019	0.8648 ± 0.012	<b>0.8665</b> ± 0.009	0.2858 ± 0.092	0.3082 ± 0.068	0.1445 ± 0.020
spectral_radius		0.3301 ± 0.016	0.3812 ± 0.030	0.7030 ± 0.010	0.7010 ± 0.019	0.8619 ± 0.013	0.8629 ± 0.009	0.6589 ± 0.021	0.6493 ± 0.023	0.8166 ± 0.004
spectral_radius_real		0.3353 ± 0.015	0.3851 ± 0.030	0.7041 ± 0.010	0.7023 ± 0.020	0.8620 ± 0.013	0.8631 ± 0.009	<b>0.6607</b> ± 0.022	<b>0.6512</b> ± 0.023	0.8077 ± 0.004
spectral_norm		0.3244 ± 0.016	0.3764 ± 0.031	0.7004 ± 0.010	0.6989 ± 0.019	0.8607 ± 0.014	0.8616 ± 0.009	0.6553 ± 0.022	0.6453 ± 0.024	0.8138 ± 0.004
weight		0.3347 ± 0.015	0.3848 ± 0.030	0.7046 ± 0.010	0.7026 ± 0.019	0.8627 ± 0.013	0.8637 ± 0.009	0.6544 ± 0.043	0.6353 ± 0.070	<b>0.8382</b> ± 0.005
tiny-imagenet		min_eig	0.2124 ± 0.052	0.1872 ± 0.061	0.2844 ± 0.059	0.2542 ± 0.087	0.3737 ± 0.095	0.3599 ± 0.093	0.5278 ± 0.037	0.5571 ± 0.046
	min_eig_real	0.1850 ± 0.054	0.1610 ± 0.062	0.2734 ± 0.065	0.2384 ± 0.079	0.3334 ± 0.095	0.3321 ± 0.101	0.4756 ± 0.040	0.5126 ± 0.051	0.1902 ± 0.023
	det	0.6407 ± 0.007	0.6367 ± 0.016	0.8132 ± 0.007	0.8127 ± 0.008	0.9070 ± 0.006	<b>0.9051</b> ± 0.009	<b>0.8095</b> ± 0.023	<b>0.7990</b> ± 0.017	0.7642 ± 0.009
	det_gram	<b>0.6411</b> ± 0.008	<b>0.6368</b> ± 0.015	<b>0.8137</b> ± 0.008	<b>0.8138</b> ± 0.007	<b>0.9077</b> ± 0.006	0.9041 ± 0.009	0.8090 ± 0.023	0.7978 ± 0.019	0.7780 ± 0.008
	spectral_radius	0.6352 ± 0.008	0.6294 ± 0.016	0.8104 ± 0.008	0.8121 ± 0.007	0.9073 ± 0.005	0.9039 ± 0.010	0.7985 ± 0.024	0.7873 ± 0.023	0.8594 ± 0.003
	spectral_radius_real	0.6317 ± 0.008	0.6297 ± 0.017	0.8050 ± 0.011	0.8018 ± 0.015	0.9033 ± 0.009	0.9016 ± 0.011	0.8017 ± 0.023	0.7887 ± 0.021	0.8435 ± 0.004
	spectral_norm	0.6336 ± 0.008	0.6276 ± 0.016	0.8094 ± 0.008	0.8113 ± 0.008	0.9068 ± 0.005	0.9035 ± 0.010	0.7952 ± 0.024	0.7825 ± 0.024	0.8498 ± 0.001
	weight	0.6364 ± 0.008	0.6309 ± 0.016	0.8110 ± 0.008	0.8128 ± 0.007	0.9076 ± 0.005	0.9044 ± 0.010	0.8085 ± 0.018	0.7983 ± 0.017	<b>0.8678</b> ± 0.002

**Table 4**  
The average compression score of each heuristic across multiple models, datasets and initializations.

1. weight	0.7786
2. spectral_radius	0.7743
3. spectral_radius_real	0.7728
4. spectral_norm	0.7707
5. det_gram	0.6831
6. det	0.6261
7. min_eig	0.3574
8. min_eig_real	0.3377

where the complex eigenvalue  $\lambda = a + bi$ . Moreover, when we only consider the real parts of the eigenvalues, their or-

dering may change which means, for instance, min\_eig may target  $\lambda_1$  whereas min\_eig\_real targets  $\lambda_2$  for the same kernel, where  $|\lambda_1| < |\lambda_2|$  but  $|a_1| > |a_2|$ .

Naturally, to be able to test the hypothesis mentioned earlier, we need to have a significant amount of complex eigenvalues in our CNNs. In Tables 5 and 6, we show the ratio of complex eigenvalues from three angles: (1) how many complex eigenvalues values do we have? ( $\frac{\# \text{ of complex eigvals}}{\# \text{ of total eigvals}}$ ), (2) how many complex eigenvalues are **targeted** by the relevant compression modes? ( $\frac{\# \text{ of targeted complex eigvals}}{\# \text{ of targeted total eigvals}}$ ), and (3) how many **pruned** kernels are deemed unimportant by looking at complex eigenvalues? ( $\frac{\# \text{ of pruned kernels using complex eigvals}}{\# \text{ of pruned kernels}}$ ).

For ResNet50,  $1 \times 1$  kernels overweight the picture. In Table 5, we see that the amount of complex eigenvalues in



**Table 5**  
Amount of total/targeted/pruned complex eigenvalues in ResNet50 for different inits

	model	total complex ratio	min_eig		min_eig_real		spectral_radius		spectral_radius_real	
			target	pruned	target	pruned	target	pruned	target	pruned
C-10	random_init	0.09 ± 0.001	0.03 ± 0.000	0.03 ± 0.000	0.04 ± 0.000	0.04 ± 0.000	0.03 ± 0.000	0.03 ± 0.000	0.02 ± 0.000	0.02 ± 0.000
	imagenet_init	0.08 ± 0.002	0.02 ± 0.000	0.03 ± 0.000	0.03 ± 0.001	0.04 ± 0.001	0.03 ± 0.001	0.03 ± 0.001	0.02 ± 0.000	0.02 ± 0.000
C-100	random_init	0.06 ± 0.002	0.02 ± 0.000	0.02 ± 0.001	0.02 ± 0.001	0.03 ± 0.001	0.01 ± 0.001	0.01 ± 0.001	0.01 ± 0.000	0.01 ± 0.001
	imagenet_init	0.07 ± 0.001	0.02 ± 0.000	0.02 ± 0.000	0.03 ± 0.000	0.03 ± 0.000	0.02 ± 0.000	0.02 ± 0.000	0.01 ± 0.000	0.01 ± 0.000
t-img	random_init	0.09 ± 0.001	0.03 ± 0.000	0.03 ± 0.000	0.04 ± 0.000	0.04 ± 0.001	0.03 ± 0.000	0.03 ± 0.001	0.02 ± 0.000	0.02 ± 0.000
	imagenet_init	0.09 ± 0.000	0.03 ± 0.000	0.03 ± 0.000	0.04 ± 0.000	0.04 ± 0.000	0.03 ± 0.000	0.03 ± 0.000	0.02 ± 0.000	0.02 ± 0.000

ResNet50 are quite small compared to thin ResNets since the  $1 \times 1$  kernels do not have any complex eigenvalues. Therefore, for complex vs. real analysis, we decided to focus on thin ResNets.

For thin ResNets, total amount of complex eigenvalues range from 30% to 40% consistently across different models, which is enough to affect the overall classification performance (Table 6). However, the total complex/real ratio may not be quite informative since different eigenvalue-based compression modes focus on different eigenvalues. For example, if the smallest absolute eigenvalues of all kernels are real and all the largest ones are complex, min\_eig and spectral\_radius may cause significantly different behavior in terms of vanilla modes vs. real value based counterparts. Hence, we include a category called **target** which indicates the amount of complex values evaluated by each compression mode whether they lead to pruning or not. According to Table 6, there is indeed a significant difference in sets of targeted values by vanilla and real value based modes, and this observation is true for both min\_eig and spectral\_radius. Thus, when we check the results in Table 3, we see that min\_eig\_real has a noticeable disadvantage against min\_eig. Nevertheless, spectral\_radius remains stable whether we choose to focus only on real values or not. This, of course, holds no importance if we did not prune any kernel due to its complex eigenvalue in the first place. Therefore, we also show the overall contribution of complex eigenvalues to the pruning. The fact that 20% – 40% of the pruned kernels are selected by looking at complex values demonstrates that there were indeed enough room for a significant change in pruning performance between vanilla and real-part-only modes (Section 6).

At the end, we see that ignoring the complex parts leads to worse performance for min\_eig mode whereas it has no significant effect on the performance of spectral\_radius mode. However, since min\_eig has already started to prune essential kernels, it is no surprise that min\_eig\_real prunes even more essential kernels. This is not the case for spectral\_radius, so we may suspect **the largest scaling factor** is more relevant for kernel importance assignment. Although the generality of this heuristic is not guaranteed, it may be useful for practitioners who want to push the pruning ratio as much as possible without losing too much recognition performance.

## 8. Set Analysis

In this section, we examine the sets of kernels pruned by each compression mode and their intersections. In our experiments, for all datasets, models, and initializations, there are only 10 distinct sets of kernels which are pruned by:

1. (min\_eig, weight, det, spectral\_radius, spectral\_norm, det\_gram)
2. (min\_eig, weight, det, spectral\_radius, det\_gram)
3. (min\_eig, weight, det, det\_gram)
4. (min\_eig, det, spectral\_radius, det\_gram)
5. (min\_eig, det, det\_gram)
6. (min\_eig, det\_gram)
7. (min\_eig, weight)
8. (min\_eig, det)
9. min\_eig
10. weight

Except 5 cases: (1,2) ResNet50 and ResNet56 for CIFAR-100 using static\_init, (3) ResNet32 for tiny-imagenet using random\_init, and (4) ResNet50 for tiny-imagenet using imagenet\_init. These cases also have kernels pruned by (min\_eig, det, spectral\_radius). In addition, (5) we may also observe kernels pruned only by det\_gram due to numerical instability born out of dealing with very small numbers.

We can draw several conclusions from these sets:

- The kernels pruned by spectral norm forms the subset of all other sets, so it is the safest heuristic among others:

$$S_{\min\_eig} \cap S_{\text{weight}} \cap S_{\text{det}} \cap S_{\text{spectral\_radius}} \cap S_{\text{det\_gram}} = S_{\text{spectral\_norm}}$$

- The extremums created by the modes based on the largest and smallest absolute eigenvalues, reflect themselves as:

$$S_{\min\_eig} \supset S_{\text{det}} \supset S_{\text{spectral\_radius}}$$

- The numerical instability mentioned in Section 6 prevents  $S_{\text{det}}$  and  $S_{\text{det\_gram}}$  to be identical. Moreover, due to the existence of (min\_eig, det) and (min\_eig, det\_gram), one is not a subset of the other either:

$$S_{\text{det}} \neq S_{\text{det\_gram}}$$

$$S_{\text{det}} \not\supset S_{\text{det\_gram}}$$

$$S_{\text{det\_gram}} \not\supset S_{\text{det}}$$

**Table 6**  
Amount of total/targeted/pruned complex eigenvalues in thin ResNets

	model	total complex ratio	min_eig		min_eig_real		spectral_radius		spectral_radius_real	
			target	pruned	target	pruned	target	pruned	target	pruned
C-10	ResNet32	0.36 ± 0.002	0.25 ± 0.002	0.27 ± 0.003	0.36 ± 0.003	0.39 ± 0.003	0.28 ± 0.003	0.33 ± 0.003	0.17 ± 0.002	0.20 ± 0.002
	ResNet56	0.39 ± 0.001	0.27 ± 0.001	0.28 ± 0.002	0.39 ± 0.002	0.41 ± 0.002	0.31 ± 0.001	0.34 ± 0.001	0.19 ± 0.001	0.21 ± 0.001
	ResNet110	0.41 ± 0.001	0.28 ± 0.001	0.29 ± 0.001	0.41 ± 0.002	0.42 ± 0.002	0.33 ± 0.001	0.34 ± 0.001	0.20 ± 0.001	0.21 ± 0.001
C-100	ResNet32	0.31 ± 0.002	0.22 ± 0.001	0.24 ± 0.002	0.31 ± 0.001	0.37 ± 0.003	0.24 ± 0.004	0.34 ± 0.005	0.14 ± 0.002	0.21 ± 0.001
	ResNet56	0.37 ± 0.002	0.25 ± 0.001	0.28 ± 0.001	0.37 ± 0.002	0.41 ± 0.002	0.29 ± 0.002	0.34 ± 0.001	0.17 ± 0.001	0.21 ± 0.001
	ResNet110	0.40 ± 0.001	0.28 ± 0.001	0.29 ± 0.001	0.41 ± 0.002	0.43 ± 0.001	0.32 ± 0.001	0.34 ± 0.001	0.19 ± 0.001	0.21 ± 0.000
t-img	ResNet32	0.35 ± 0.003	0.24 ± 0.002	0.26 ± 0.004	0.35 ± 0.003	0.39 ± 0.004	0.27 ± 0.003	0.32 ± 0.002	0.16 ± 0.001	0.19 ± 0.002
	ResNet56	0.39 ± 0.002	0.27 ± 0.004	0.28 ± 0.003	0.39 ± 0.003	0.41 ± 0.002	0.31 ± 0.001	0.33 ± 0.003	0.18 ± 0.001	0.20 ± 0.001
	ResNet110	0.41 ± 0.001	0.28 ± 0.001	0.28 ± 0.001	0.41 ± 0.001	0.42 ± 0.001	0.32 ± 0.001	0.33 ± 0.001	0.19 ± 0.001	0.20 ± 0.001

Another outcome of this numerical problem:

$$S_{\text{det\_gram}} \not\approx S_{\text{spectral\_radius}}$$

- We can see the distinction between weight-based pruning and eigenvalue-based pruning:

$$S_{\text{min\_eig}} \not\approx S_{\text{weight}}$$

$$S_{\text{weight}} \not\approx \{S_{\text{min\_eig}}, S_{\text{det}}, S_{\text{spectral\_radius}}, S_{\text{det\_gram}}\}$$

Additional information, such as the ratio of each set with respect to the union of all sets, and the variance of these ratios across multiple runs can be found in Appendix A.

### 9. Pruning per Layer

Summary of findings:

- Dataset has a footprint over the activity map ( $\frac{\text{\# of active params}}{\text{total \# of params}}$ ) of a CNN.
- Thin ResNet experiments show that, within the same model family, activity maps of different models resemble each other.
- ResNet50 experiments show that significantly different initializations affect the activity map.
- For randomly initialized models, first layers have relatively smaller pruning ratio than the deeper layers.

In this section, we study how pruning affects different layers. In Fig 3, we show the amount of activity ( $\frac{\text{\# of active params}}{\text{total \# of params}}$ ) in different layers of different models of thin ResNet family. Considering the similarity of overall activity pattern, we see that **the dataset at hand has a footprint over the pruned architecture**. In detail, row-wise similarity is relatively low (same model - different dataset) whereas column-wise similarity indicates a correlation of activity patterns of different models from the same family for the same dataset. Of course, as the model gets smaller (ResNet32) activity of the first layers gets higher than that of larger models (ResNet56 and ResNet110). Nevertheless, it is interesting to see **aligned spikes in activity**, for example the spike at layers: ResNet32:25 - ResNet56:40 - ResNet110:80 on CIFAR-100, since these

alignments require the stretch of activities over layers for different models where the number of layers are significantly different. However, generalization of this behavior is restricted within a somewhat vague model family definition (thin ResNets) as ResNet50 does not exhibit the same overall activity pattern. It seems using fundamental building blocks (thin ResNet block) to generate shallow/deep models leads to interesting activity distributions which may be used to study the importance/effect of depth in neural nets from a different perspective. Another factor that affects the activity pattern is initialization. We show this effect in Fig 4. CNN training contains different sources of randomness that can affect the results. Hence, we include static\_init results to compare with random\_init results to show how little these perturbations are in our experiments. Nevertheless, the key observation here is that **significantly different initializations** (imagenet\_init vs. random\_init) **results in different activity patterns**. In addition, imagenet\_init is the only case where we observe a drop in first layers’ activities. On the other hand, with the exception of sudden increase in last layer activities on tiny\_imagenet, we see a general proclivity towards low activity in last layers, but the exact reason for this phenomenon and its generality to different datasets/models remains an open question.

### 10. Pruning through Epochs

Summary of findings:

- The first drop in learning rate is found to be a very interesting turning point for pruning:
  - The difference between the min and the max abs eigenvalues of 3×3 kernels starts to increase. As a result, the heuristics that use the former starts to prune more and suffer in classification performance.
  - The pruning ratios of all heuristics starts to increase until they reach approximately the same amount of pruning. Nevertheless, as the training continues the min abs eigenvalue based heuristics eventually reach higher pruning ratios.

Here, we decided on the number of epochs (200) by looking at the learning curves of multiple experiments. Our pol-

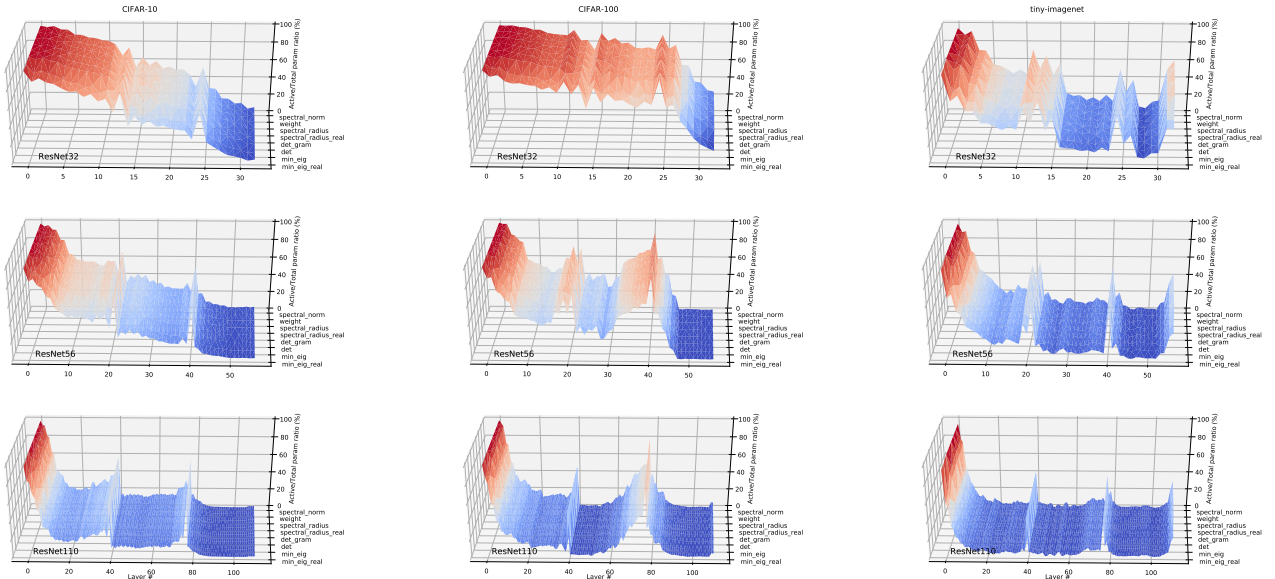


Figure 3: Active parameter ratio of different compression modes through layers (input → output) for thin ResNets under multiple random initializations.

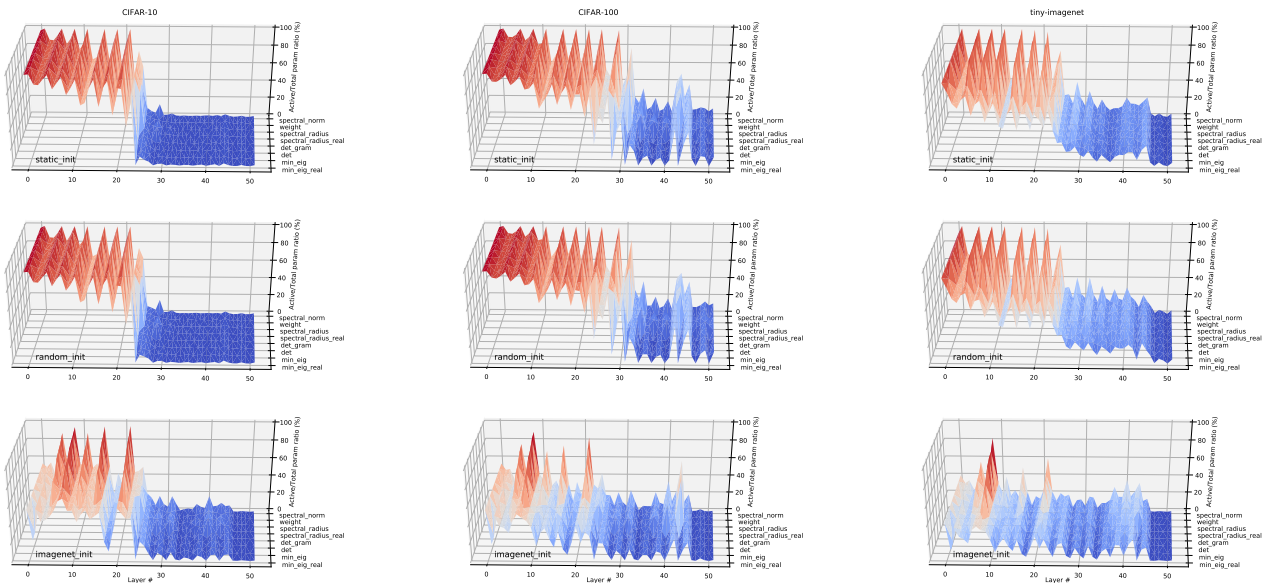


Figure 4: Active parameter ratio of different compression modes through layers (input → output) for ResNet50 under different initializations.

icy was to keep training for a while after the learning curve became nearly flat. However, recently, training history gained more importance due to interesting observations such as *epoch-wise double descent* [53]. Hence, after every 10 epochs, we **simulated** pruning for each compression mode as if it was the end of the training to construct a **pruning history**. Using this history, we ask two questions: (1) What would we see if we stopped the training at an earlier stage? (2) Can we use compression score to estimate the utilization of a given model’s capacity, then for example to use it to decide whether to stop the training or not?

In Fig 5 and Fig 7, we show pruning ratio of each compression mode through epochs. As expected (see Sections 6, 8, and 7), *min\_eig\_real* always prunes the most (Fig 6 and Fig 8). The interesting observation here is that, for thin ResNets, other compression modes almost catches up *min\_eig* in terms of pruning ratio after 90<sup>th</sup> epoch which is right after we divide the learning rate by 10 (80<sup>th</sup> epoch). This is not the case for ResNet50 where the curves are quite similar to each other and the gap between them is never as big as in the thin ResNet case. However, ResNet50 contains a significant amount of  $1 \times 1$  kernels (no difference between compression

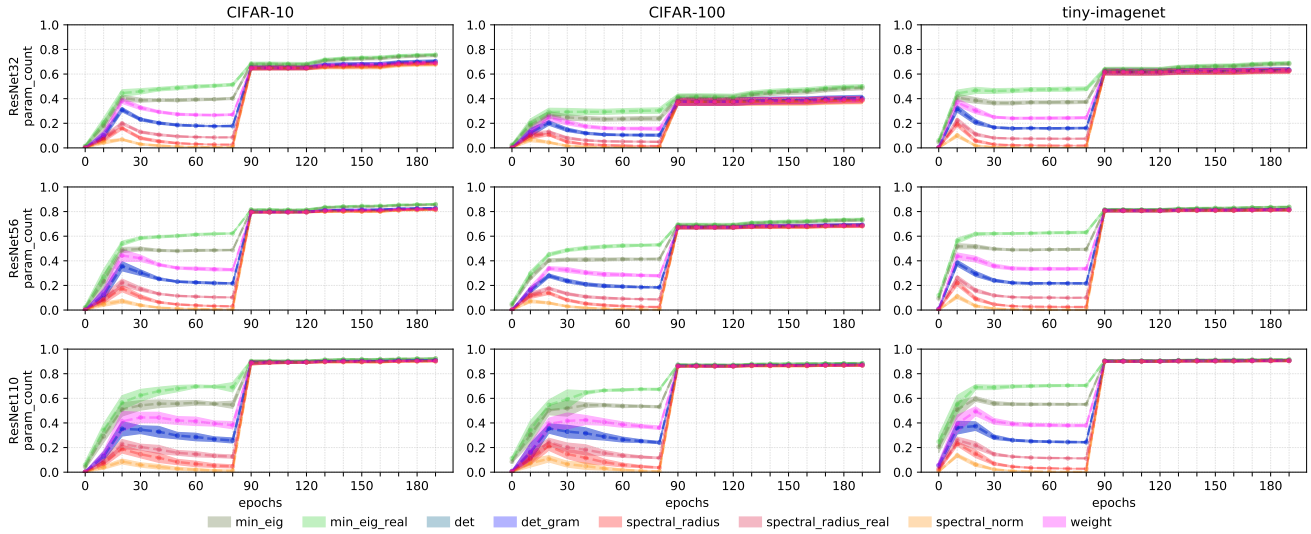


Figure 5: Pruning ratios of different thin ResNets through epochs for different datasets.

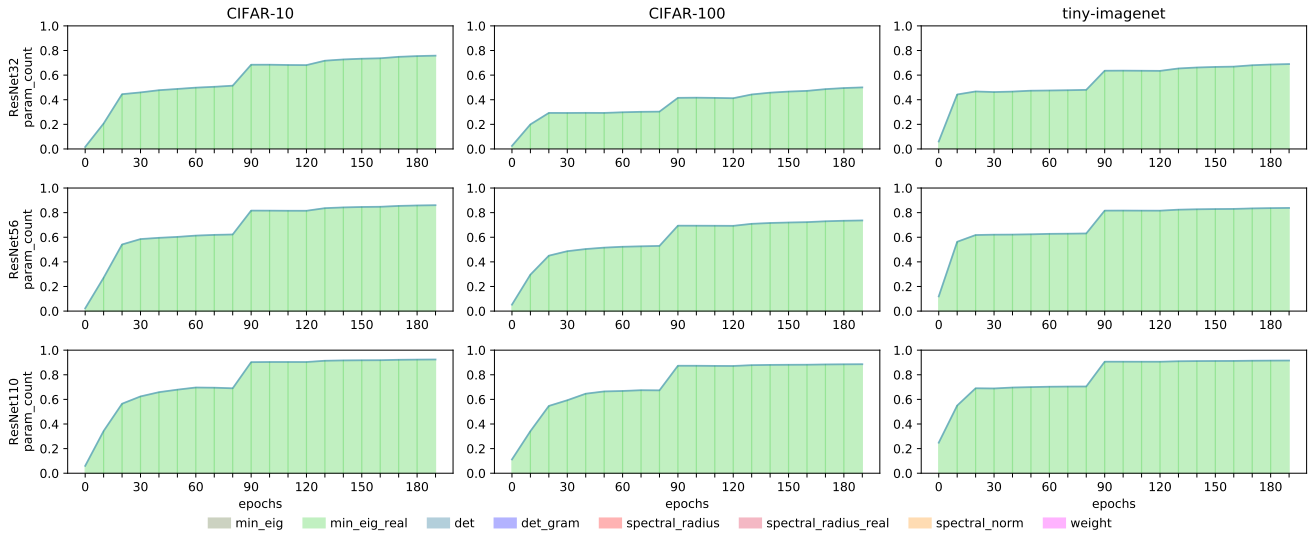


Figure 6: min\_eig\_real always achieves the best pruning ratio for different thin ResNets through epochs using different datasets.

modes), so it is expected for different modes to draw similar curves.

In Fig 9, we show classification accuracy of each compression mode through epochs for different thin ResNets. In comparison to pruning ratio charts, classification performances vary significantly which results in indistinguishable results for the first 90 epochs. However, after that point, there is a strong divergence in performance for min\_eig and min\_eig\_real whereas other modes continue to perform quite similarly. This similarity is shown in Fig 10 where the color of the best mode in the previous simulation point is reflected by painting the next 10 epoch interval. Note that det and det\_gram can also diverge from the red-ish curve depending on the eigenvalue distribution, and we observe this probability in Fig 11 as the blue-ish curves also diverge from

the red-ish ones in later stages of training. As in the thin ResNet case, we see frequent changes in the mode with the best recognition performance in Fig 12.

Compression score (see Section 6) combines the opposing forces in model compression: (1) pruning ratio, (2) classification accuracy. For thin ResNets, this combination manifests itself very clearly: in Fig 13, (1) for the first 80 epochs curves are aligned and clearly distinguishable as in Fig 5, then they merge between epochs 80 - 90, (2) after 90<sup>th</sup> epoch green curves (min\_eig and min\_eig\_real) diverges from the rest as in Fig 9. In addition, ResNet50 also follows this pattern though with greater perturbation (Fig 15). We again see three main clusters of lines: red, blue, green. They go relatively aligned at first as in Fig 7, then diverge as in Fig 11. Which compression mode is at the top? The ones with the

## A Deeper Look into Convolutions via Pruning

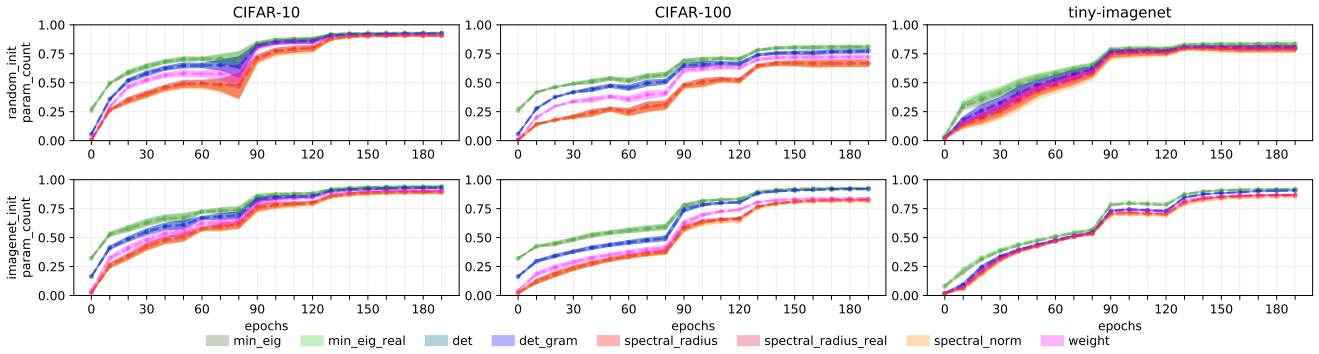


**Figure 7:** Pruning ratios of ResNet50 through epochs for different datasets under different initializations.

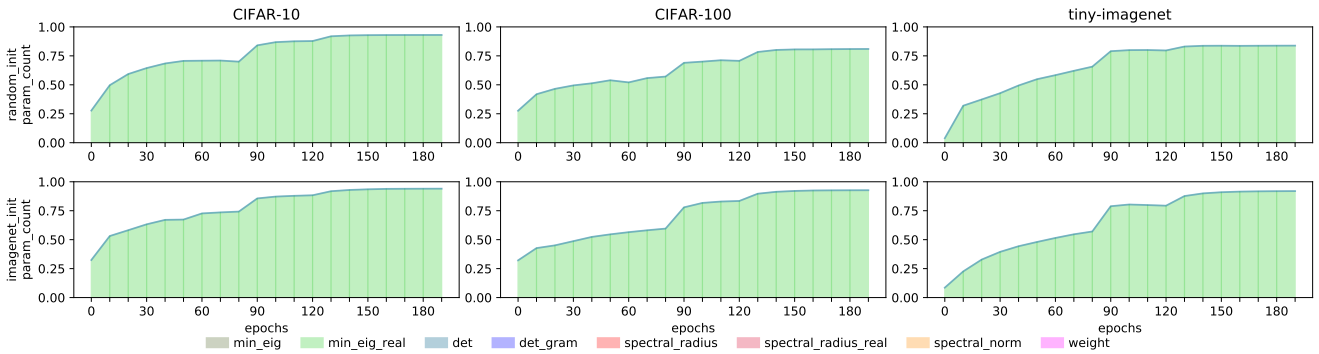


**Figure 8:** `min_eig_real` always achieves the best pruning ratio for ResNet50 through epochs under different initializations.

highest compression score at the different stages of training are shown in Fig 14 and Fig 16. According to these results, winners change frequently and do not follow a general pattern. Hence, we evaluate winner based comparison not as

informative as the clusters-of-modes analysis.

In overall, we found an interesting point of behavioral change in pruning, epoch 80. **After the first drop in learning rate, we identified an interesting shift in the eigen-**

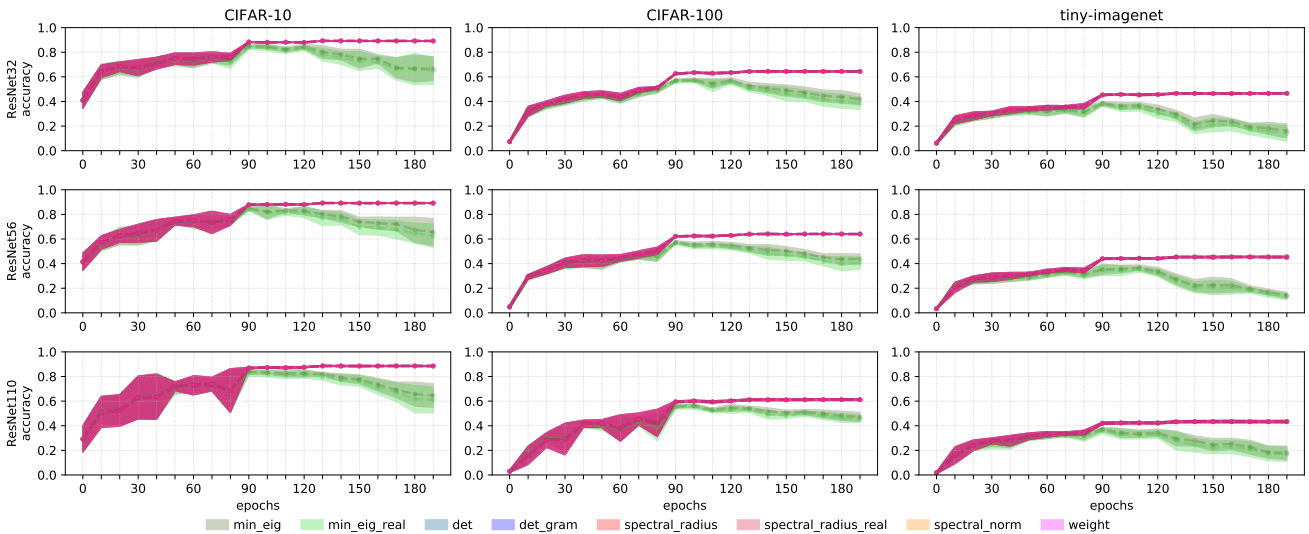


**Figure 9:** Classification accuracy of different thin ResNets through epochs for different datasets.

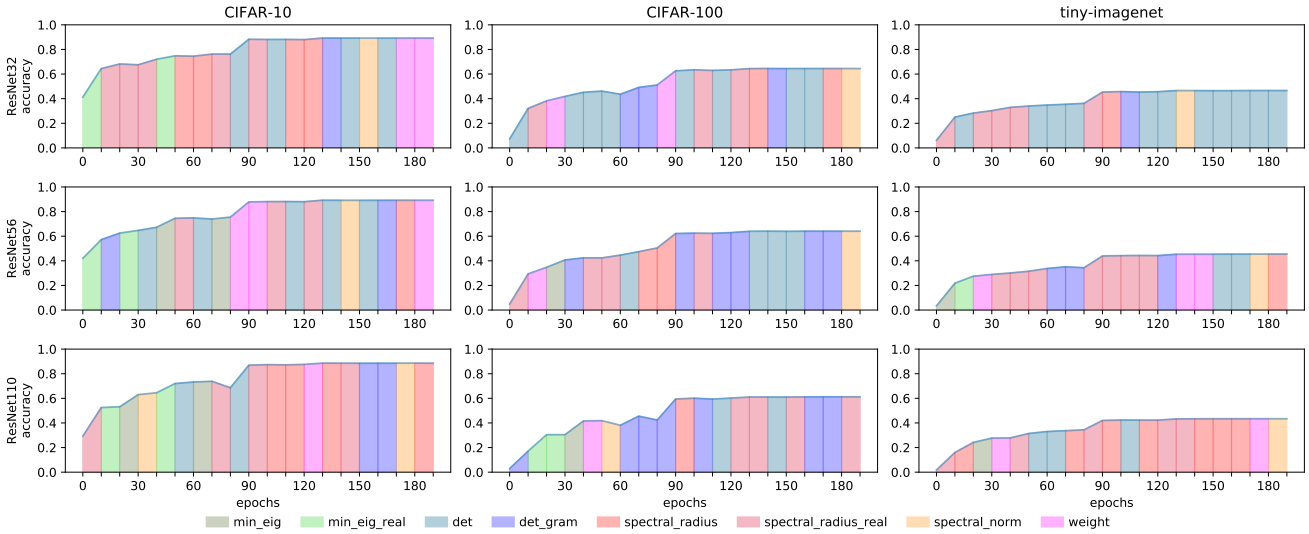


Figure 10: Compression modes with the best classification accuracy through epochs for thin ResNets.

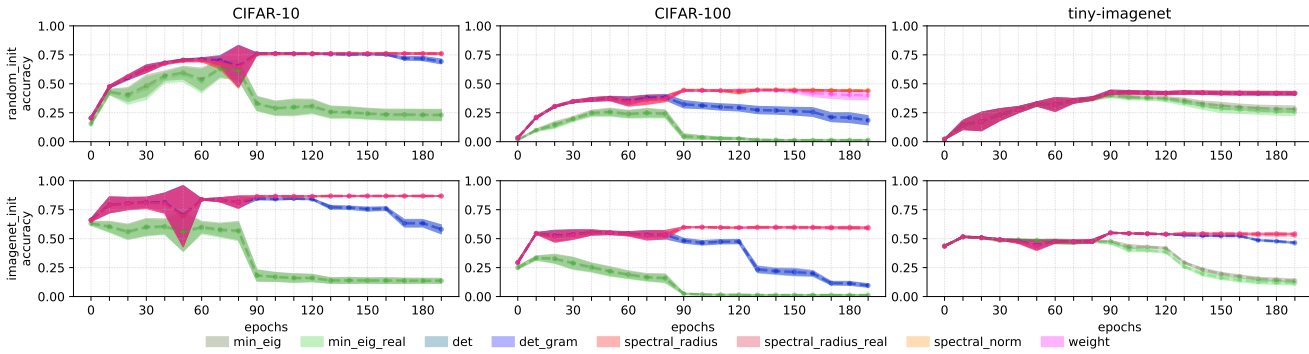


Figure 11: Classification accuracy of ResNet50 through epochs for different datasets under different initializations.

value distribution resulting in (1) convergence of different modes' compression scores, then (2) divergence of minimum absolute eigenvalue based modes. Why is this important? Nakkiran et al. [53] note that if one has a large

enough model they can observe an epoch-wise double descent where the training is split into two halves with different behaviors. This two stage learning model also resembles the information bottleneck principle [61] and the critical

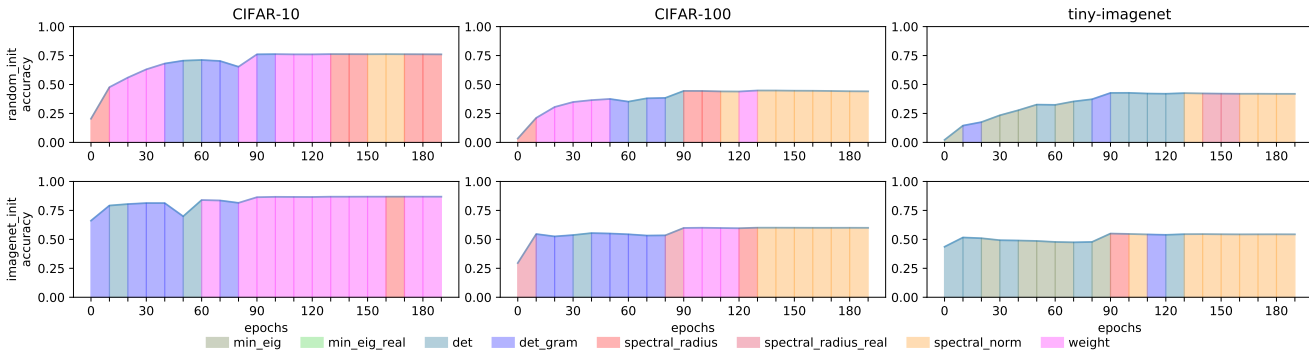
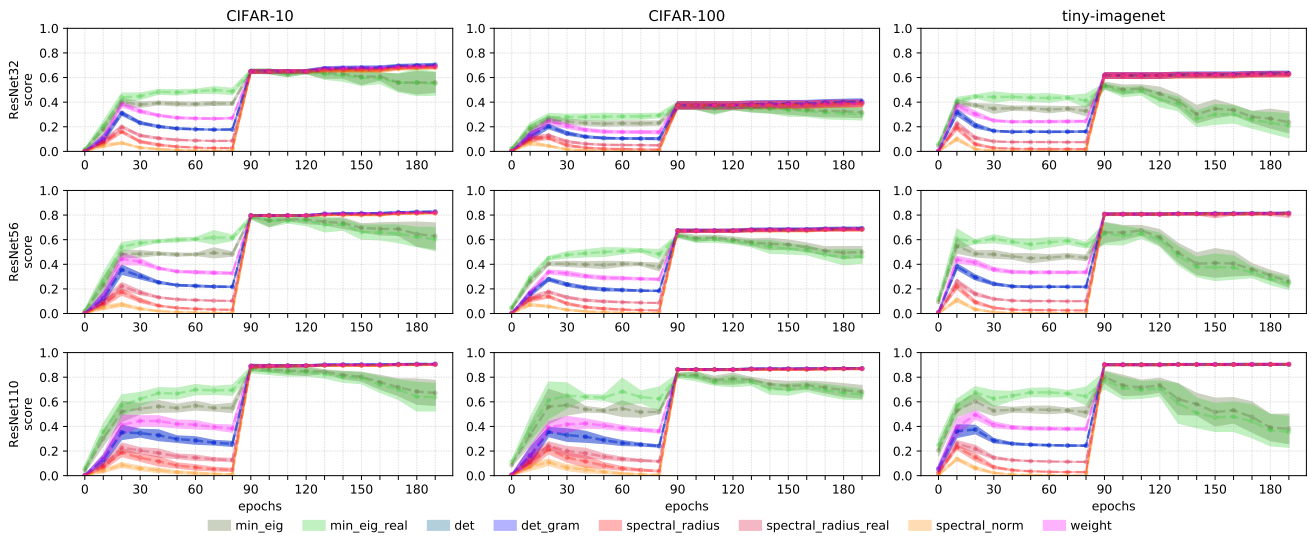
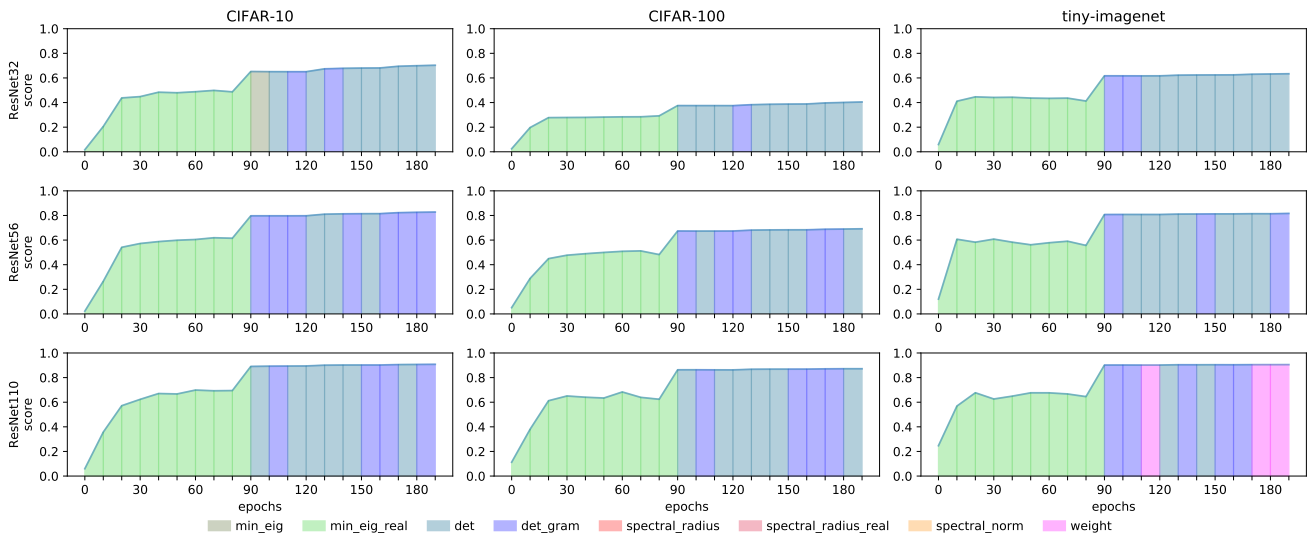


Figure 12: Compression modes with the best classification accuracy through epochs for ResNet50 under different initializations.

## A Deeper Look into Convolutions via Pruning



**Figure 13:** Compression score of different thin ResNets through epochs for different datasets.



**Figure 14:** Compression modes with the best compression score through epochs for thin ResNets.

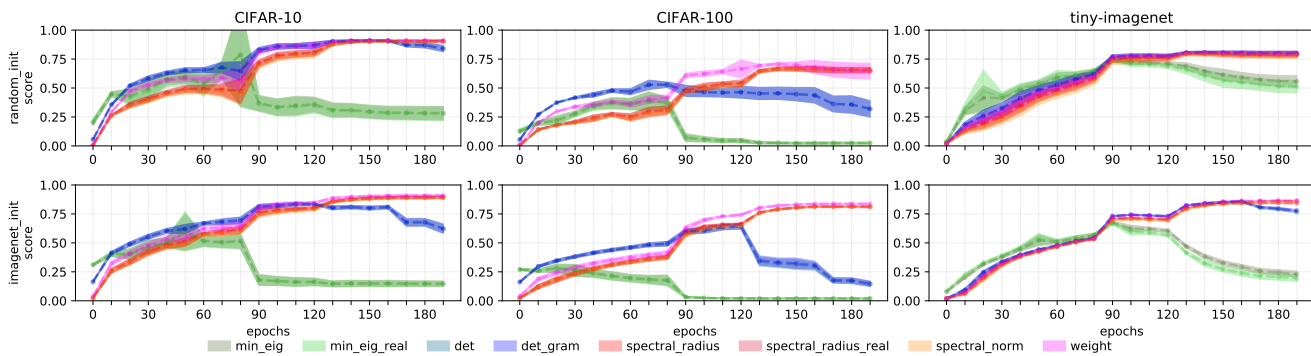


**Figure 15:** Compression score of ResNet50 through epochs for different datasets under different initializations.

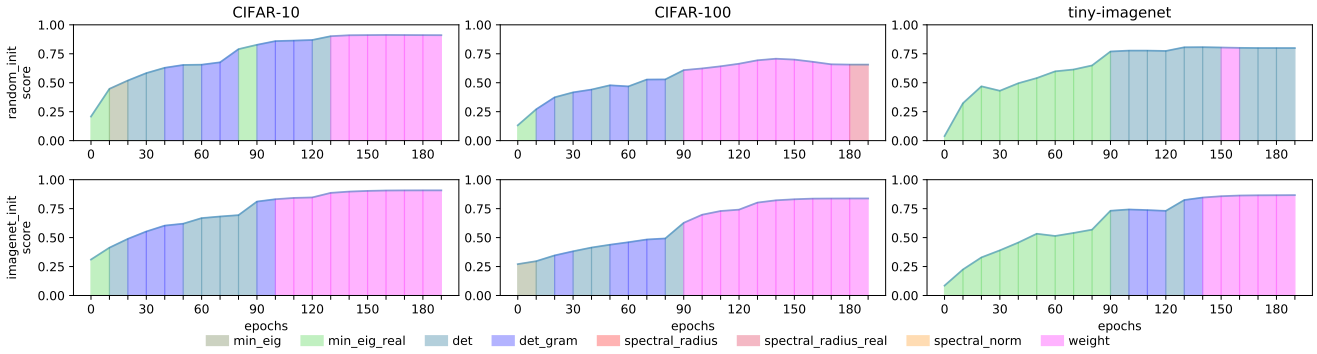


Figure 16: Compression modes with the best compression score through epochs for ResNet50 under different initializations.

learning period [2]. It seems that, in deep learning literature, the two phased learning is observed again and again in different concepts. Although, we cannot explain the behavior of the eigenvalues in our experiments, it is important to report this incident since each new observation of the **two stage learning** model decreases the odds of experiencing a mere coincidence. Hence, we leave extensive study on the relationship between eigenvalues and the learning rate that resulted in the two phases shown in Figs 13 and 15 as a future work.

### 11. Discussion

We can also find the expert kernels in human brain. It is well known that adult brain contains special modules that activate for specific functions such as face recognition [34]. What is more interesting for us is that these experts emerge from a natural pruning phase [9]: "In normal development, the pathway for each eye is sculpted (or "pruned") down to the right number of connections, and those connections are sculpted in other ways, for example, to allow one to see patterns. By overproducing synapses then selecting the right connections, the brain develops an organized wiring diagram that functions optimally." A clear example is given by Haier et al. [21, 20] where it is shown that high brain activity while learning to play Tetris is replaced by a low brain activity once the subjects reach a certain level of expertise in the game. The authors of these papers state that the correlation between improvement on the task and decreasing brain glucose use suggests that those who honed their cognitive strategy to the fewest circuits improved the most. In fact, these studies are part of a wider picture known as the **neural efficiency hypothesis of intelligence** [54, 56]. Hence, we think pruning is imperative to understand the learning dynamics of convolutional neural nets.

In addition, while trying to set the optimal  $L_1$  regularization penalty,  $\alpha = 4 * 10^{-4}$  and  $\alpha = 10^{-5}$  experiments revealed an interesting phenomenon. In general, model compression consists of 3 phases: (1) training with regularization, (2) pruning, (3) fine-tuning without (excessive) regularization. Although we do not use the fine-tuning phase in our analysis, we, nonetheless, also run fine-tuning trials in

our preliminary experiments, and observed opposite effects for  $4 * 10^{-4}$  and  $10^{-5}$ . In our experiments, excessive pruning with  $4 * 10^{-4}$  damages the model capacity in such a way that fine-tuning actually decreases the performance of the model whereas  $10^{-5}$  selection can still benefit from fine-tuning. Nevertheless, this observation requires a detailed study focused entirely on pruning vs. model capacity, so we leave this as a future work.

### 12. Conclusions and Future Work

In this work, we study matrix characteristics for pruning in an attempt to answer the question: what is an expert kernel? In this pursuit, we found that (1) spectral norm is a more robust heuristic (in the sense that it better preserves generalization accuracy) than the average absolute weight for pruning, (2) one can use spectral radius of a kernel as a useful heuristic for pruning and push the compression ratio by discarding the complex parts of the eigenvalues while preserving the recognition performance, (3) a kernel can be essential whether it is full-rank or not, (4) theoretical pruning heuristics may not hold in practice due to numerical instabilities born out of dealing with very small numbers, (5) datasets have a significant footprint in the activity map (active parameter distribution across layers after pruning) of a model family in a homogeneous  $L_1$  regularization (each layer has the same regularization penalty), (6) the gap between the smallest and the largest eigenvalue of a kernel starts to increase after the first drop in the learning rate which resulted in a divergence of compression scores achieved by minimum and maximum absolute eigenvalue based pruning heuristics. With these in mind, we leave extensive study on neural activity through layers, two stages of eigenvalue distributions and their connection to the learning rate for future research.



## References

- [1] Abel, N.H., 1826. Beweis der unmöglichkeit, algebraische gleichungen von höheren graden als dem vierten allgemein aufzulösen. *Journal für die reine und angewandte Mathematik* 1, 65–84.
- [2] Achille, A., Rovere, M., Soatto, S., 2018. Critical learning periods in deep networks, in: *International Conference on Learning Representations*.
- [3] Arora, S., Ge, R., Neyshabur, B., Zhang, Y., 2018. Stronger generalization bounds for deep nets via a compression approach, in: *International Conference on Machine Learning*, pp. 254–263.
- [4] Baykal, C., Liebenwein, L., Gilitschenski, I., Feldman, D., Rus, D., 2018. Data-dependent coresets for compressing neural networks with applications to generalization bounds, in: *International Conference on Learning Representations*.
- [5] Behrmann, J., Grathwohl, W., Chen, R.T., Duvenaud, D., Jacobsen, J.H., 2019. Invertible residual networks, in: *International Conference on Machine Learning*, pp. 573–582.
- [6] Belkin, M., Hsu, D., Ma, S., Mandal, S., 2019. Reconciling modern machine-learning practice and the classical bias–variance trade-off. *Proceedings of the National Academy of Sciences* 116, 15849–15854.
- [7] Blakeney, C., Yan, Y., Zong, Z., 2020. Is pruning compression?: Investigating pruning via network layer similarity, in: *The IEEE Winter Conference on Applications of Computer Vision*, pp. 914–922.
- [8] Chollet, F., 2015. keras.
- [9] Council, N.R., et al., 2000. How people learn: Brain, mind, experience, and school: Expanded edition. National Academies Press.
- [10] Dong, X., Chen, S., Pan, S., 2017. Learning to prune deep neural networks via layer-wise optimal brain surgeon, in: *Advances in Neural Information Processing Systems*, pp. 4857–4867.
- [11] Dubey, A., Chatterjee, M., Ahuja, N., 2018. Coreset-based neural network compression, in: *Proceedings of the European Conference on Computer Vision (ECCV)*, pp. 454–470.
- [12] Frankle, J., Carbin, M., 2018. The lottery ticket hypothesis: Finding sparse, trainable neural networks, in: *International Conference on Learning Representations*.
- [13] Fukushima, K., Miyake, S., 1982. Neocognitron: A self-organizing neural network model for a mechanism of visual pattern recognition, in: *Competition and cooperation in neural nets*. Springer, pp. 267–285.
- [14] Galois, É., Neumann, P.M., 2011. The mathematical writings of Évariste Galois. volume 6. European Mathematical Society.
- [15] Gerschgorin, S., 1931. Über die abgrenzung der eigenwerte einer matrix. *Izvestija Akademii Nauk SSSR, Serija Matematika* 7, 749–754.
- [16] Goodfellow, I., Bengio, Y., Courville, A., 2016. Deep learning.
- [17] Goodfellow, I., Pouget-Abadie, J., Mirza, M., Xu, B., Warde-Farley, D., Ozair, S., Courville, A., Bengio, Y., 2014. Generative adversarial nets, in: *Advances in neural information processing systems*, pp. 2672–2680.
- [18] Gordon, A., Eban, E., Nachum, O., Chen, B., Wu, H., Yang, T.J., Choi, E., 2018. Morphnet: Fast & simple resource-constrained structure learning of deep networks, in: *Proceedings of the IEEE conference on computer vision and pattern recognition*, pp. 1586–1595.
- [19] Guo, Y., Yao, A., Chen, Y., 2016. Dynamic network surgery for efficient dnns, in: *Advances in neural information processing systems*, pp. 1379–1387.
- [20] Haier, R.J., Siegel, B., Tang, C., Abel, L., Buchsbaum, M.S., 1992a. Intelligence and changes in regional cerebral glucose metabolic rate following learning. *Intelligence* 16, 415–426.
- [21] Haier, R.J., Siegel Jr, B.V., MacLachlan, A., Soderling, E., Lottenberg, S., Buchsbaum, M.S., 1992b. Regional glucose metabolic changes after learning a complex visuospatial/motor task: a positron emission tomographic study. *Brain research* 570, 134–143.
- [22] Han, S., Mao, H., Dally, W.J., 2016. Deep compression: Compressing deep neural networks with pruning, trained quantization and Huffman coding .
- [23] Han, S., Pool, J., Tran, J., Dally, W., 2015. Learning both weights and connections for efficient neural network, in: *Advances in neural information processing systems*, pp. 1135–1143.
- [24] Hassibi, B., Stork, D.G., 1993. Second order derivatives for network pruning: Optimal brain surgeon, in: *Advances in neural information processing systems*, pp. 164–171.
- [25] He, K., Zhang, X., Ren, S., Sun, J., 2015. Delving deep into rectifiers: Surpassing human-level performance on imagenet classification, in: *Proceedings of the IEEE international conference on computer vision*, pp. 1026–1034.
- [26] He, K., Zhang, X., Ren, S., Sun, J., 2016. Deep residual learning for image recognition, in: *Proceedings of the IEEE conference on computer vision and pattern recognition*, pp. 770–778.
- [27] He, Y., Liu, P., Wang, Z., Hu, Z., Yang, Y., 2019. Filter pruning via geometric median for deep convolutional neural networks acceleration, in: *Proceedings of the IEEE Conference on Computer Vision and Pattern Recognition*, pp. 4340–4349.
- [28] He, Y., Zhang, X., Sun, J., 2017. Channel pruning for accelerating very deep neural networks, in: *Proceedings of the IEEE International Conference on Computer Vision*, pp. 1389–1397.
- [29] Howard, A.G., Zhu, M., Chen, B., Kalenichenko, D., Wang, W., Weyand, T., Andreetto, M., Adam, H., 2017. Mobilenets: Efficient convolutional neural networks for mobile vision applications. *arXiv preprint arXiv:1704.04861* .
- [30] Huang, Z., Wang, N., 2018. Data-driven sparse structure selection for deep neural networks, in: *Proceedings of the European conference on computer vision (ECCV)*, pp. 304–320.
- [31] Iandola, F.N., Han, S., Moskewicz, M.W., Ashraf, K., Dally, W.J., Keutzer, K., 2016. Squeezenet: Alexnet-level accuracy with 50x fewer parameters and < 0.5 mb model size. *arXiv preprint arXiv:1602.07360* .
- [32] Ioffe, S., Szegedy, C., 2015. Batch normalization: Accelerating deep network training by reducing internal covariate shift, in: *International Conference on Machine Learning*, pp. 448–456.
- [33] Junjie, L., Zhe, X., Runbin, S., Cheung, R.C., So, H.K., 2020. Dynamic sparse training: Find efficient sparse network from scratch with trainable masked layers, in: *International Conference on Learning Representations*.
- [34] Kanwisher, N., McDermott, J., Chun, M.M., 1997. The fusiform face area: a module in human extrastriate cortex specialized for face perception. *Journal of neuroscience* 17, 4302–4311.
- [35] Kingma, D.P., Ba, J., 2014. Adam: A method for stochastic optimization. *arXiv preprint arXiv:1412.6980* .
- [36] Krizhevsky, A., et al., 2009. Learning multiple layers of features from tiny images .
- [37] LeCun, Y., Boser, B., Denker, J.S., Henderson, D., Howard, R.E., Hubbard, W., Jackel, L.D., 1989. Backpropagation applied to handwritten zip code recognition. *Neural computation* 1, 541–551.
- [38] LeCun, Y., Denker, J.S., Solla, S.A., 1990. Optimal brain damage, in: *Advances in neural information processing systems*, pp. 598–605.
- [39] Li, C., Farkhoor, H., Liu, R., Yosinski, J., 2018. Measuring the intrinsic dimension of objective landscapes, in: *International Conference on Learning Representations*.
- [40] Li, F.F., Karpathy, A., Johnson, J., 2017a. Tiny imagenet visual recognition challenge .
- [41] Li, H., Kadav, A., Durdanovic, I., Samet, H., Graf, H.P., 2017b. Pruning filters for efficient convnets .
- [42] Li, Y., Gu, S., Gool, L.V., Timofte, R., 2019. Learning filter basis for convolutional neural network compression, in: *Proceedings of the IEEE International Conference on Computer Vision*, pp. 5623–5632.
- [43] Lin, S., Ji, R., Yan, C., Zhang, B., Cao, L., Ye, Q., Huang, F., Doermann, D., 2019. Towards optimal structured cnn pruning via generative adversarial learning, in: *Proceedings of the IEEE Conference on Computer Vision and Pattern Recognition*, pp. 2790–2799.
- [44] Liu, Z., Li, J., Shen, Z., Huang, G., Yan, S., Zhang, C., 2017. Learning efficient convolutional networks through network slimming, in: *Proceedings of the IEEE International Conference on Computer Vision*, pp. 2736–2744.
- [45] Liu, Z., Sun, M., Zhou, T., Huang, G., Darrell, T., 2018. Rethinking the value of network pruning, in: *International Conference on Learning Representations*.

- ing Representations.
- [46] Long, J., Shelhamer, E., Darrell, T., 2015. Fully convolutional networks for semantic segmentation, in: Proceedings of the IEEE conference on computer vision and pattern recognition, pp. 3431–3440.
- [47] Luo, J.H., Wu, J., Lin, W., 2017. Thinet: A filter level pruning method for deep neural network compression, in: Proceedings of the IEEE international conference on computer vision, pp. 5058–5066.
- [48] Miyato, T., Kataoka, T., Koyama, M., Yoshida, Y., 2018. Spectral normalization for generative adversarial networks. arXiv preprint arXiv:1802.05957 .
- [49] Molchanov, P., Tyree, S., Karras, T., Aila, T., Kautz, J., 2017. Pruning convolutional neural networks for resource efficient inference.
- [50] Mozer, M.C., Smolensky, P., 1989. Skeletonization: A technique for trimming the fat from a network via relevance assessment, in: Advances in neural information processing systems, pp. 107–115.
- [51] Mpitsos, G.J., Burton Jr, R.M., 1992. Convergence and divergence in neural networks: Processing of chaos and biological analogy. Neural networks 5, 605–625.
- [52] Mussay, B., Osadchy, M., Braverman, V., Zhou, S., Feldman, D., 2019. Data-independent neural pruning via coresets, in: International Conference on Learning Representations.
- [53] Nakkiran, P., Kaplun, G., Bansal, Y., Yang, T., Barak, B., Sutskever, I., 2019. Deep double descent: Where bigger models and more data hurt. arXiv preprint arXiv:1912.02292 .
- [54] Neubauer, A.C., Fink, A., 2009. Intelligence and neural efficiency. Neuroscience & Biobehavioral Reviews 33, 1004–1023.
- [55] Nowlan, S.J., Hinton, G.E., 1992. Simplifying neural networks by soft weight-sharing. Neural computation 4, 473–493.
- [56] Nussbaumer, D., Grabner, R.H., Stern, E., 2015. Neural efficiency in working memory tasks: The impact of task demand. Intelligence 50, 196–208.
- [57] Ramakrishnan, R.K., Sari, E., Nia, V.P., 2020. Differentiable mask for pruning convolutional and recurrent networks, in: 2020 17th Conference on Computer and Robot Vision (CRV), IEEE. pp. 222–229.
- [58] Russakovsky, O., Deng, J., Su, H., Krause, J., Satheesh, S., Ma, S., Huang, Z., Karpathy, A., Khosla, A., Bernstein, M., et al., 2015. Imagenet large scale visual recognition challenge. International journal of computer vision 115, 211–252.
- [59] Sandler, M., Howard, A., Zhu, M., Zhmoginov, A., Chen, L.C., 2018. Mobilenetv2: Inverted residuals and linear bottlenecks, in: Proceedings of the IEEE conference on computer vision and pattern recognition, pp. 4510–4520.
- [60] Schwartz, R., Dodge, J., Smith, N.A., Etzioni, O., 2020. Green ai. Communications of the ACM 63, 54–63.
- [61] Shwartz-Ziv, R., Tishby, N., 2017. Opening the black box of deep neural networks via information. arXiv preprint arXiv:1703.00810 .
- [62] Sietsma, J., 1988. Neural net pruning-why and how, in: Proceedings of International Conference on Neural Networks, San Diego, CA, 1988, pp. 325–333.
- [63] Son, S., Nah, S., Mu Lee, K., 2018. Clustering convolutional kernels to compress deep neural networks, in: Proceedings of the European Conference on Computer Vision (ECCV), pp. 216–232.
- [64] Szegedy, C., Vanhoucke, V., Ioffe, S., Shlens, J., Wojna, Z., 2016. Rethinking the inception architecture for computer vision, in: Proceedings of the IEEE conference on computer vision and pattern recognition, pp. 2818–2826.
- [65] Ullrich, K., Meeds, E., Welling, M., 2017. Soft weight-sharing for neural network compression .
- [66] Wen, W., Wu, C., Wang, Y., Chen, Y., Li, H., 2016. Learning structured sparsity in deep neural networks, in: Advances in neural information processing systems, pp. 2074–2082.
- [67] Yang, T.J., Chen, Y.H., Sze, V., 2017. Designing energy-efficient convolutional neural networks using energy-aware pruning, in: Proceedings of the IEEE Conference on Computer Vision and Pattern Recognition, pp. 5687–5695.
- [68] Ye, J., Lu, X., Lin, Z., Wang, J.Z., 2018. Rethinking the smaller-norm-less-informative assumption in channel pruning of convolution layers, in: International Conference on Learning Representations.
- [69] Ye, S., Xu, K., Liu, S., Cheng, H., Lambrechts, J.H., Zhang, H., Zhou, A., Ma, K., Wang, Y., Lin, X., 2019. Adversarial robustness vs. model compression, or both?, in: Proceedings of the IEEE/CVF International Conference on Computer Vision, pp. 111–120.
- [70] Yu, R., Li, A., Chen, C.F., Lai, J.H., Morariu, V.I., Han, X., Gao, M., Lin, C.Y., Davis, L.S., 2018. Nisp: Pruning networks using neuron importance score propagation, in: Proceedings of the IEEE Conference on Computer Vision and Pattern Recognition, pp. 9194–9203.
- [71] Zhang, C., Bengio, S., Hardt, M., Recht, B., Vinyals, O., 2016. Understanding deep learning requires rethinking generalization .
- [72] Zhao, C., Ni, B., Zhang, J., Zhao, Q., Zhang, W., Tian, Q., 2019. Variational convolutional neural network pruning, in: Proceedings of the IEEE Conference on Computer Vision and Pattern Recognition, pp. 2780–2789.

## A. Appendix

Here we present the detailed results of our set analysis (see Section 8).

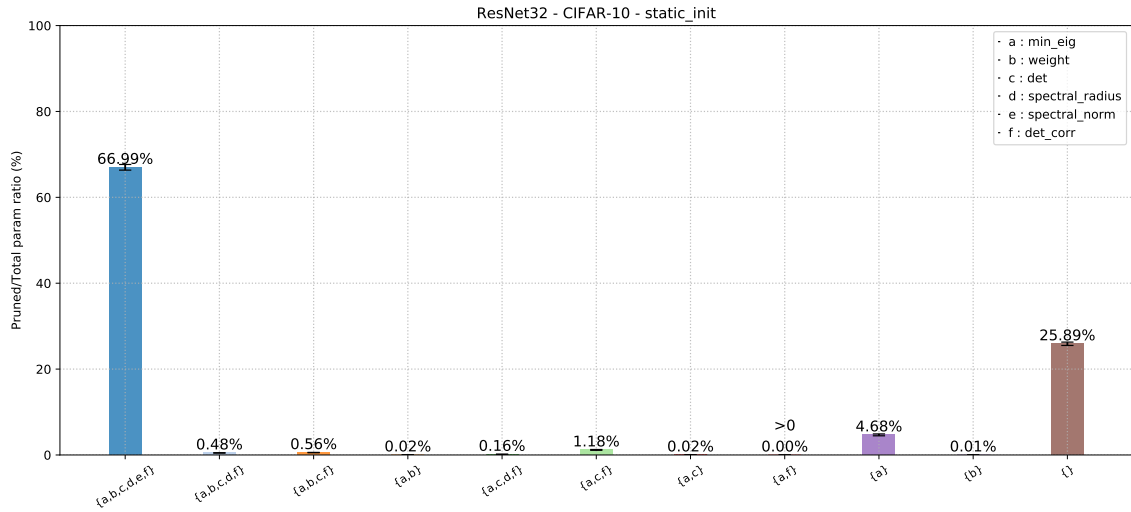


Figure 17: Set analysis bar chart for ResNet32 on CIFAR-10 with static\_init

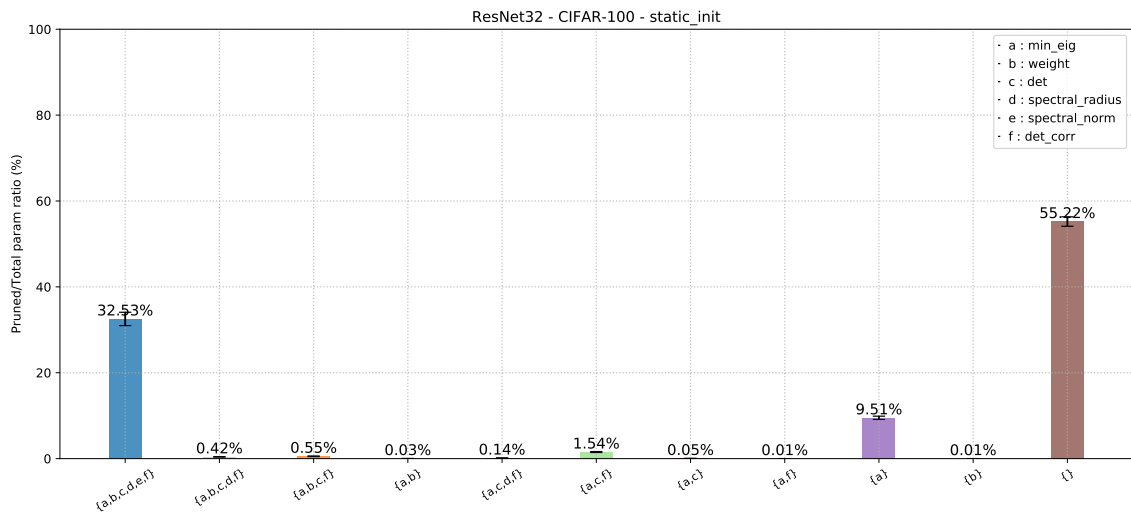
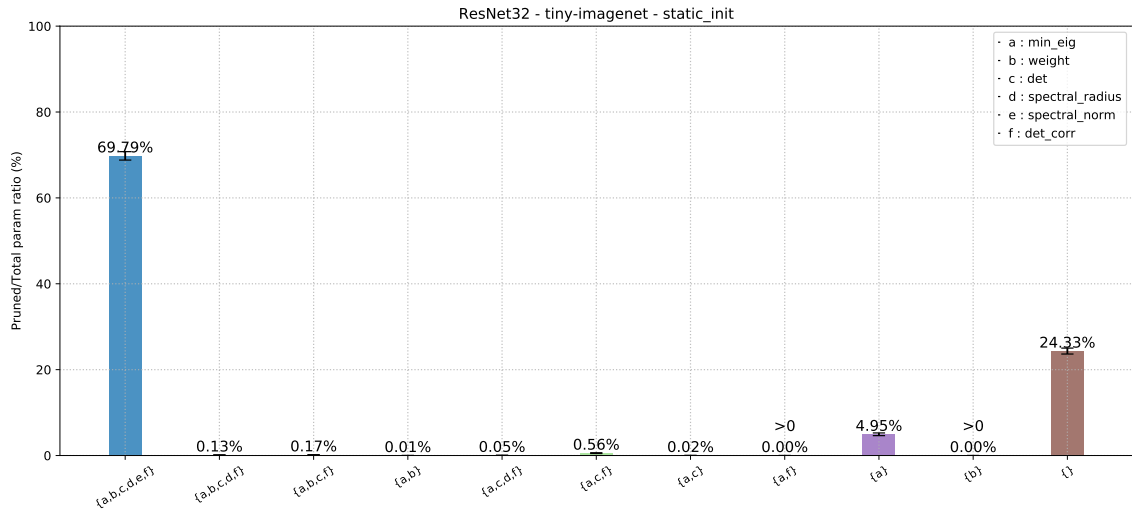
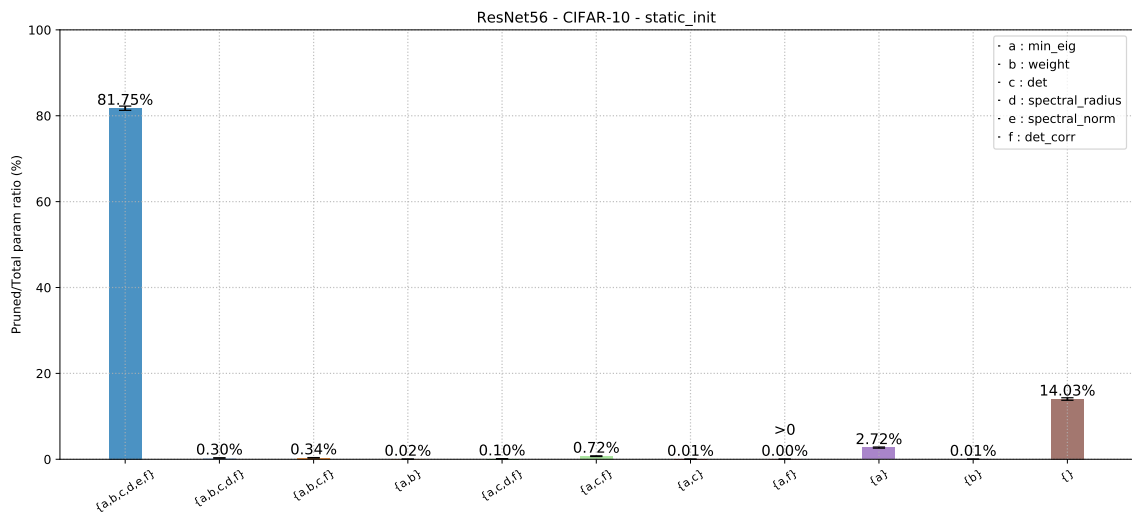


Figure 18: Set analysis bar chart for ResNet32 on CIFAR-100 with static\_init

## A Deeper Look into Convolutions via Pruning



**Figure 19:** Set analysis bar chart for ResNet32 on tiny-imagenet with static\_init



**Figure 20:** Set analysis bar chart for ResNet56 on CIFAR-10 with static\_init

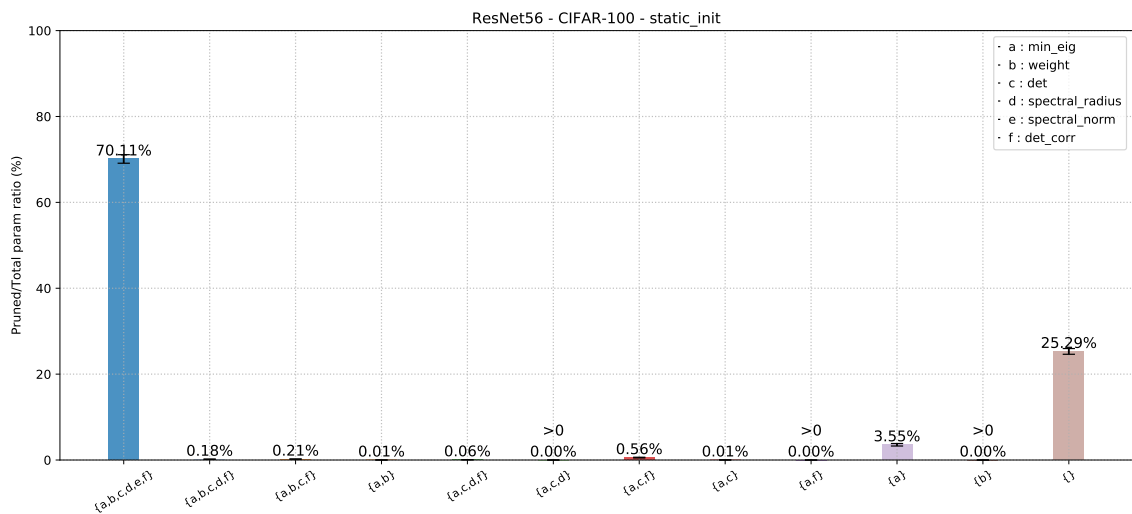


**Figure 21:** Set analysis bar chart for ResNet56 on CIFAR-100 with static\_init

## A Deeper Look into Convolutions via Pruning

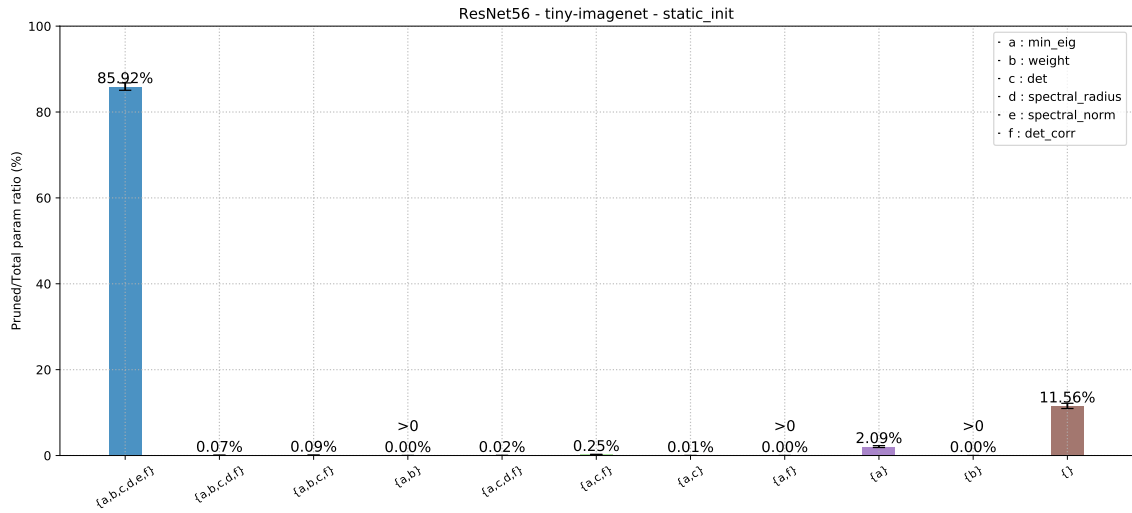


**Figure 22:** Set analysis bar chart for ResNet56 on tiny-imagenet with static\_init

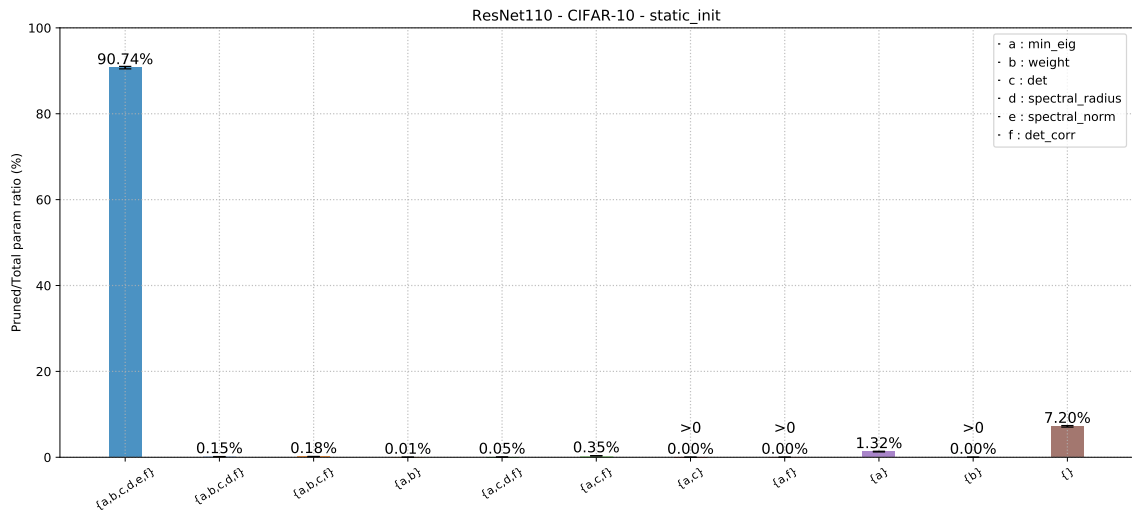


**Figure 23:** Set analysis bar chart for ResNet110 on CIFAR-10 with static\_init

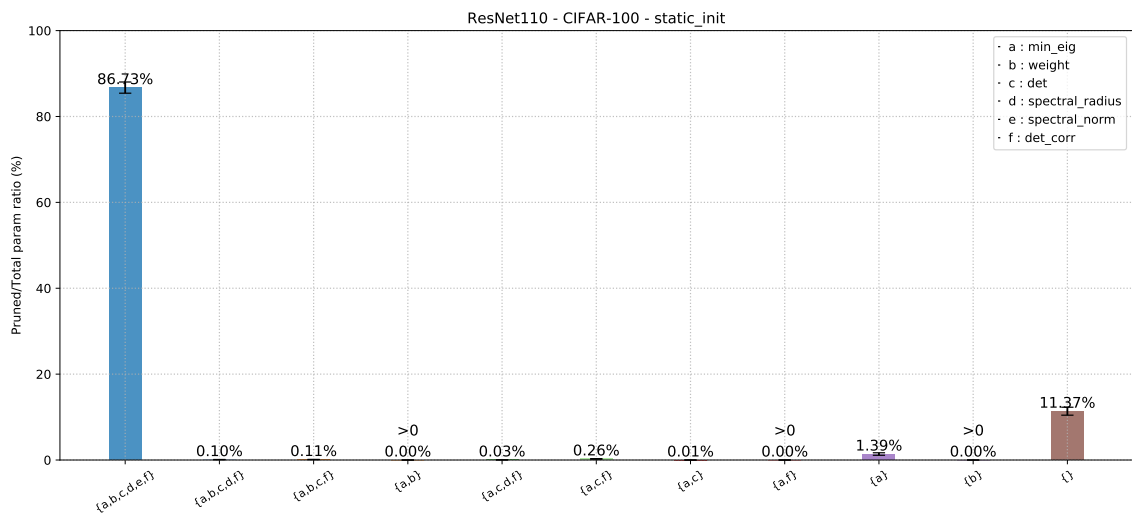


**Figure 24:** Set analysis bar chart for ResNet110 on CIFAR-100 with static\_init

## A Deeper Look into Convolutions via Pruning

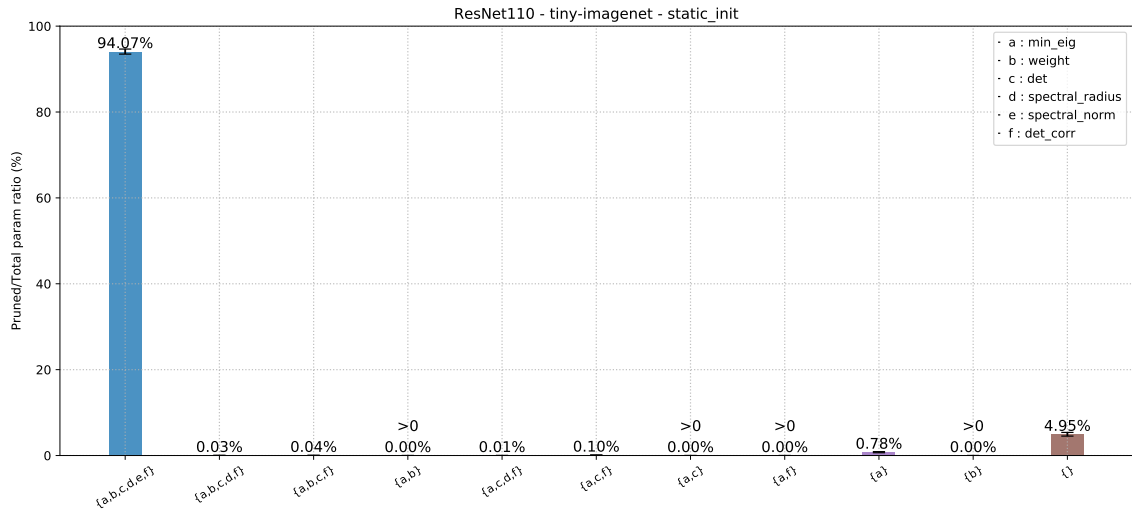


**Figure 25:** Set analysis bar chart for ResNet110 on tiny-imagenet with static\_init

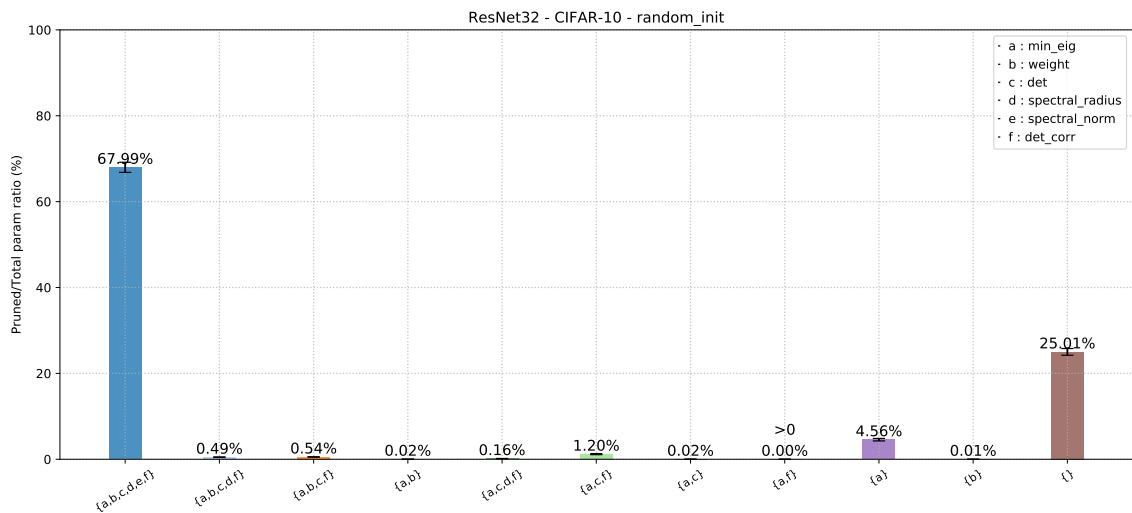


**Figure 26:** Set analysis bar chart for ResNet32 on CIFAR-10 with random\_init

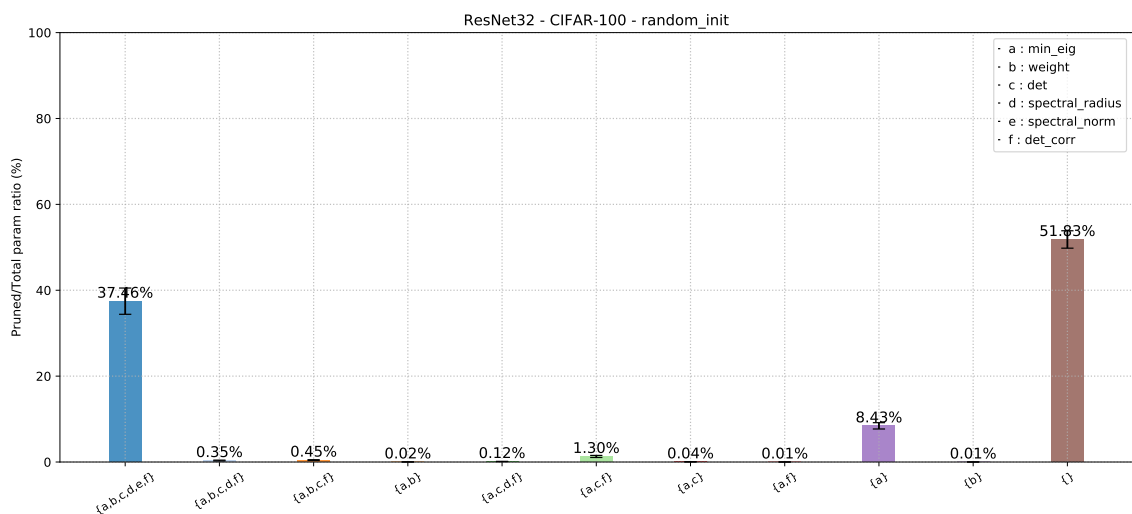


**Figure 27:** Set analysis bar chart for ResNet32 on CIFAR-100 with random\_init

## A Deeper Look into Convolutions via Pruning

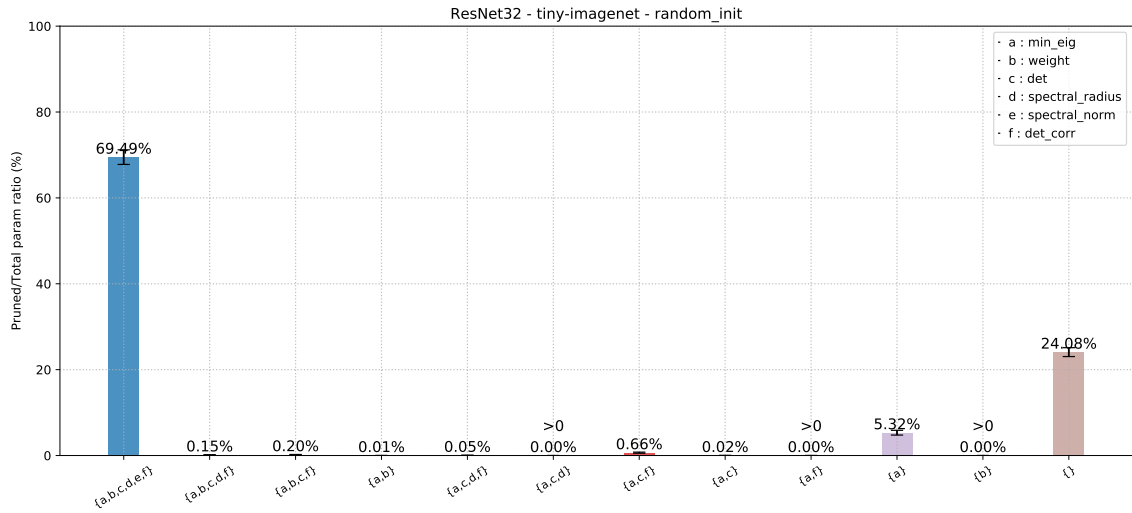


**Figure 28:** Set analysis bar chart for ResNet32 on tiny-imagenet with random\_init

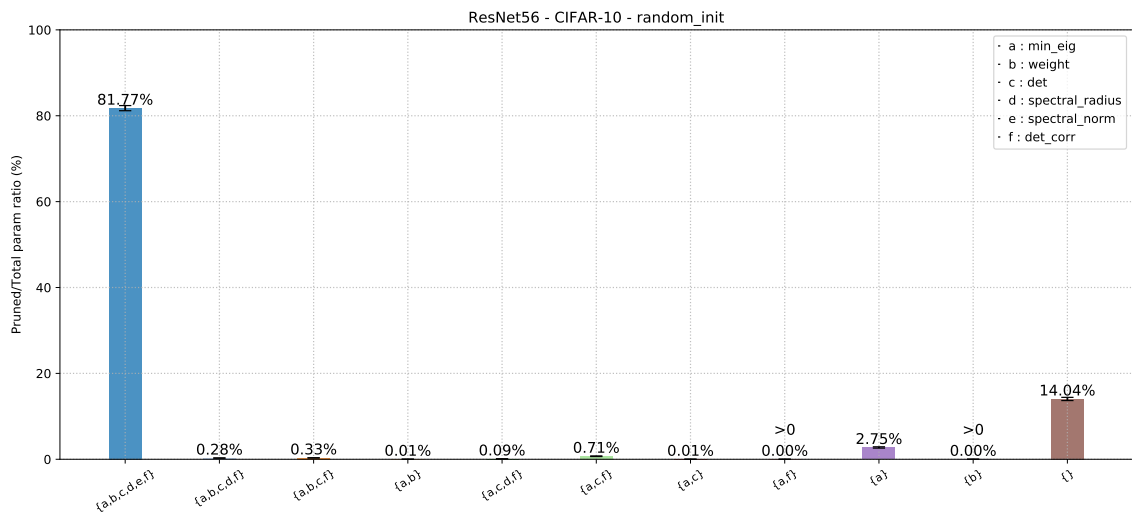


**Figure 29:** Set analysis bar chart for ResNet56 on CIFAR-10 with random\_init

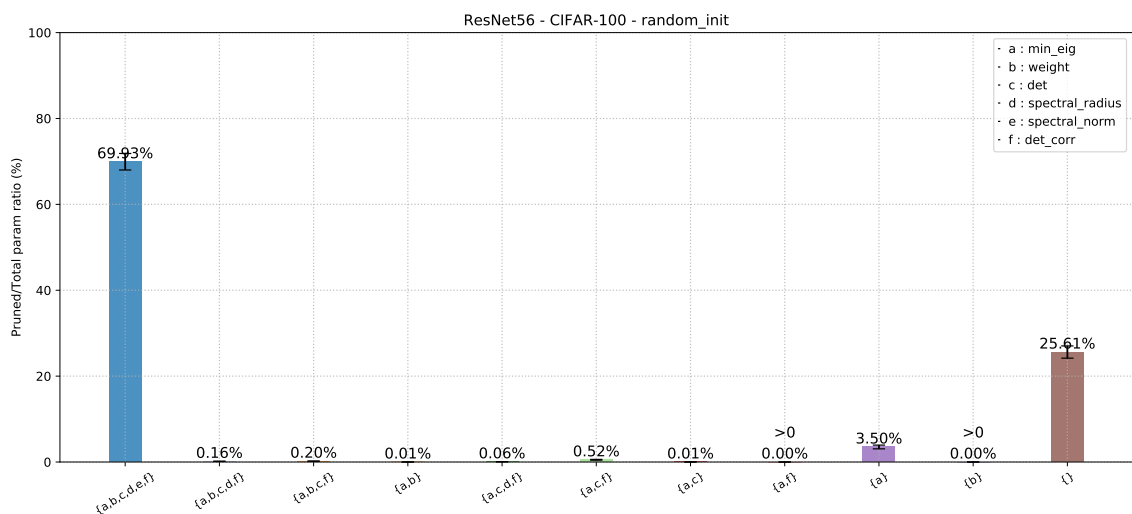


**Figure 30:** Set analysis bar chart for ResNet56 on CIFAR-100 with random\_init

## A Deeper Look into Convolutions via Pruning

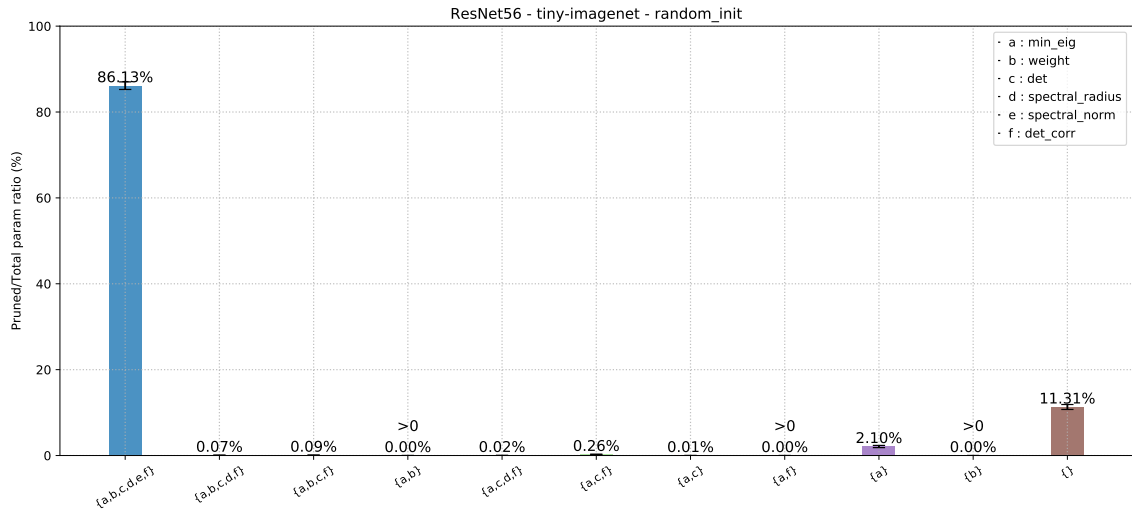


**Figure 31:** Set analysis bar chart for ResNet56 on tiny-imagenet with random\_init

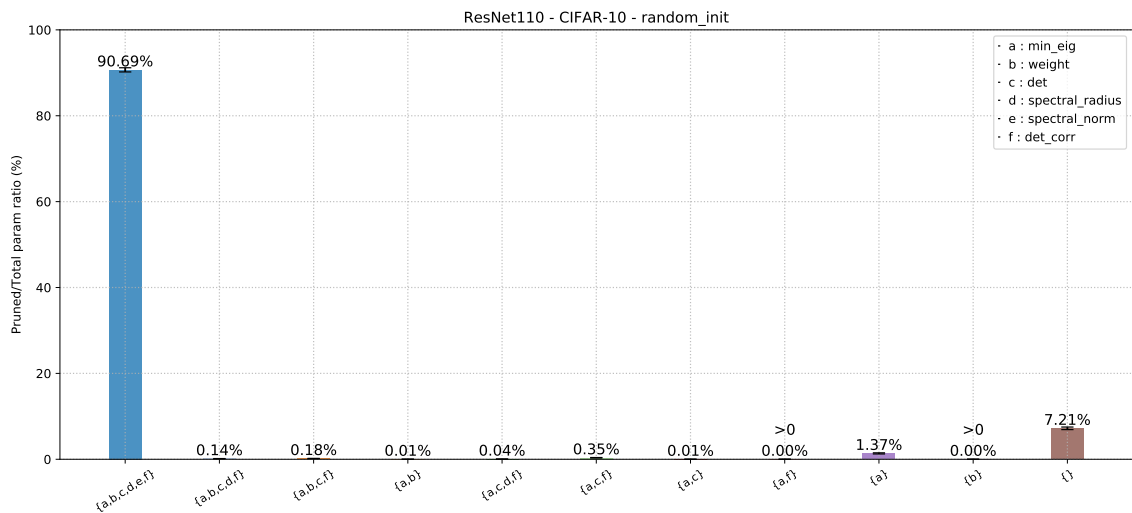


**Figure 32:** Set analysis bar chart for ResNet110 on CIFAR-10 with random\_init

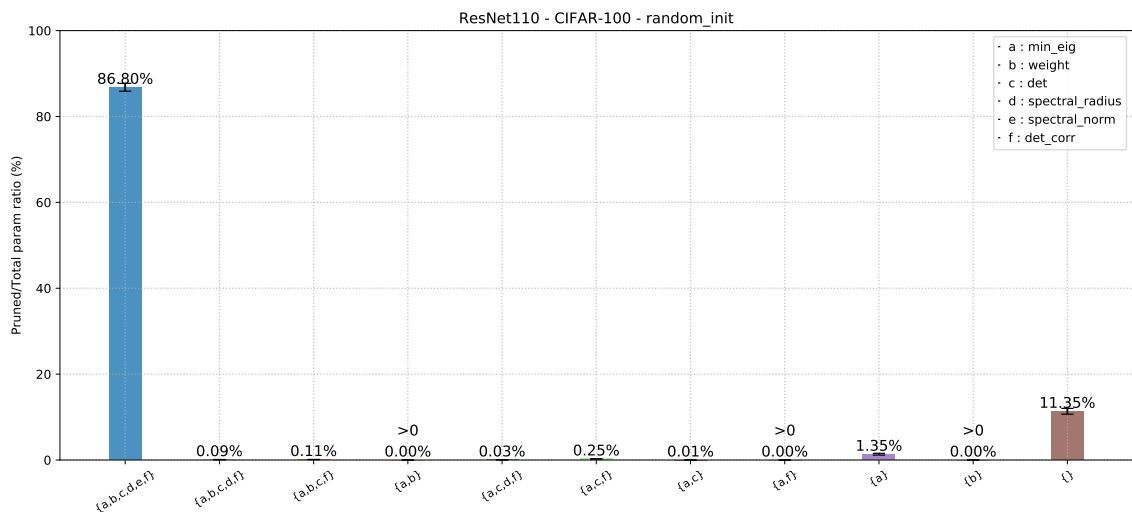


**Figure 33:** Set analysis bar chart for ResNet110 on CIFAR-100 with random\_init



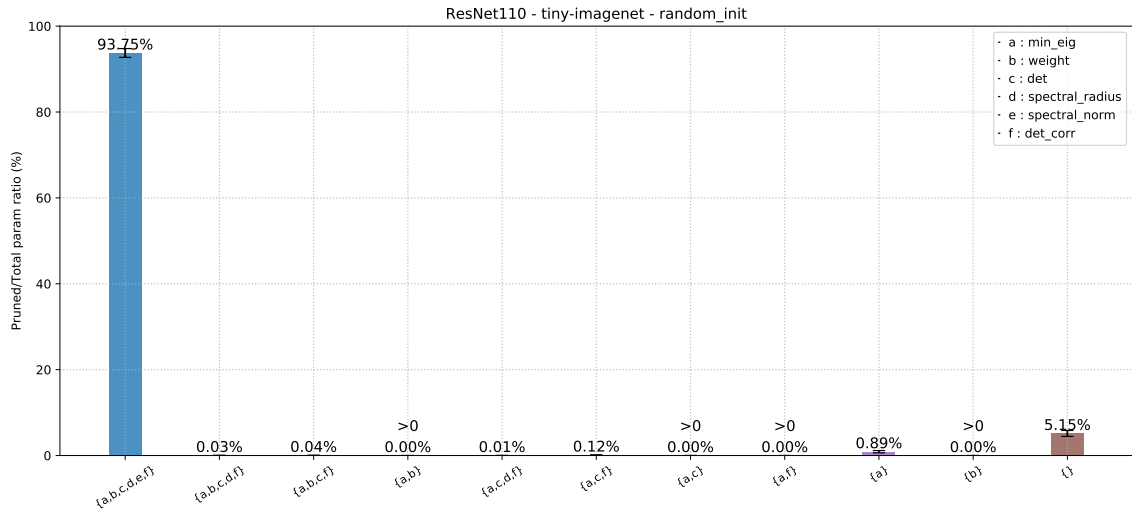


Figure 34: Set analysis bar chart for ResNet110 on tiny-imagenet with random\_init

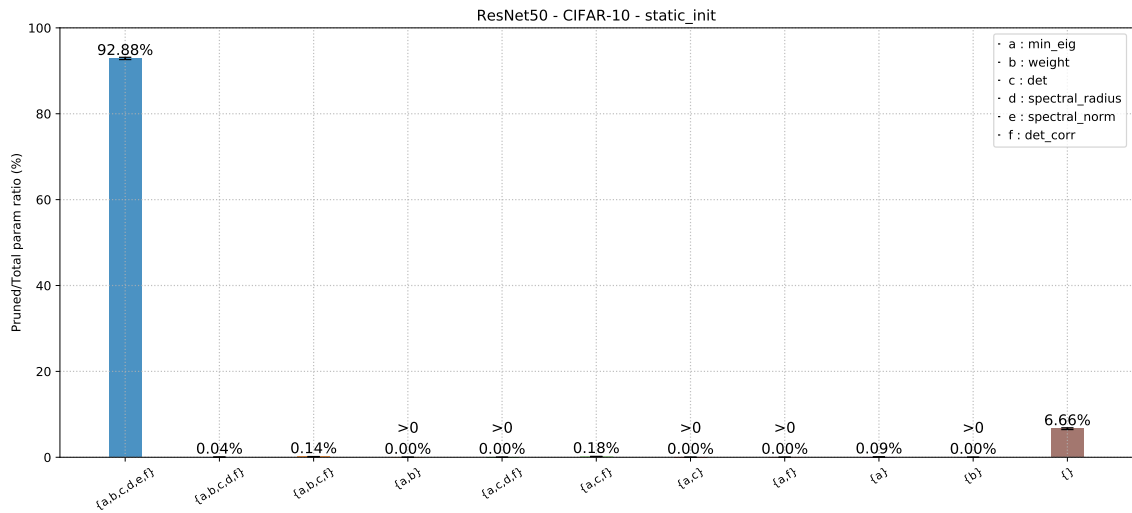


Figure 35: Set analysis bar chart for ResNet50 on CIFAR-10 with static\_init

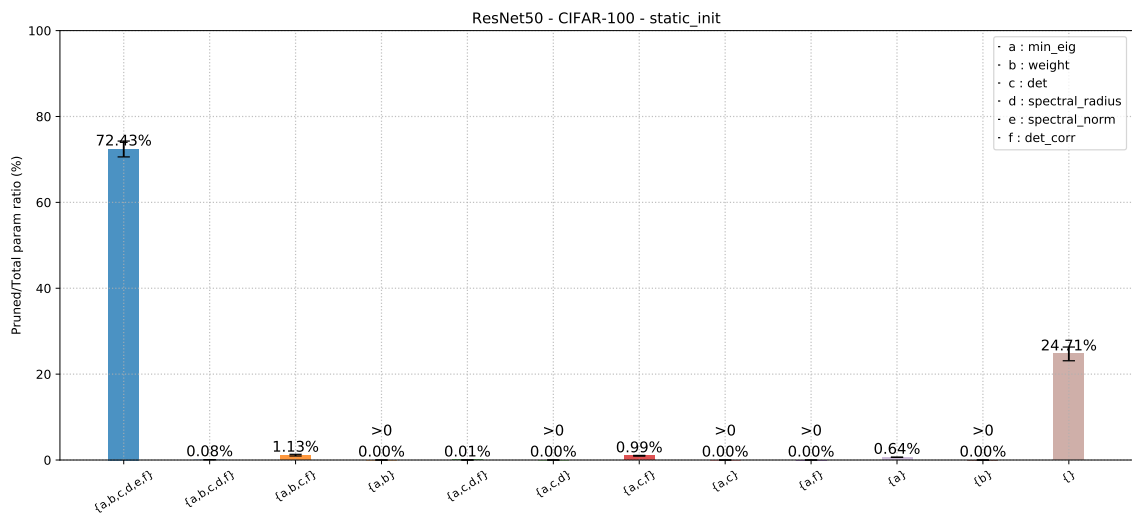
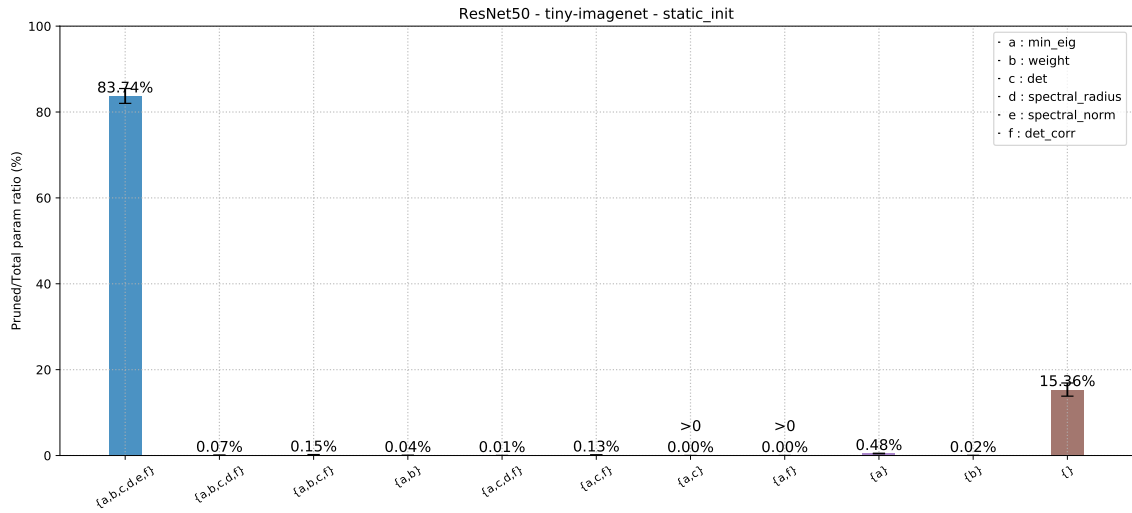
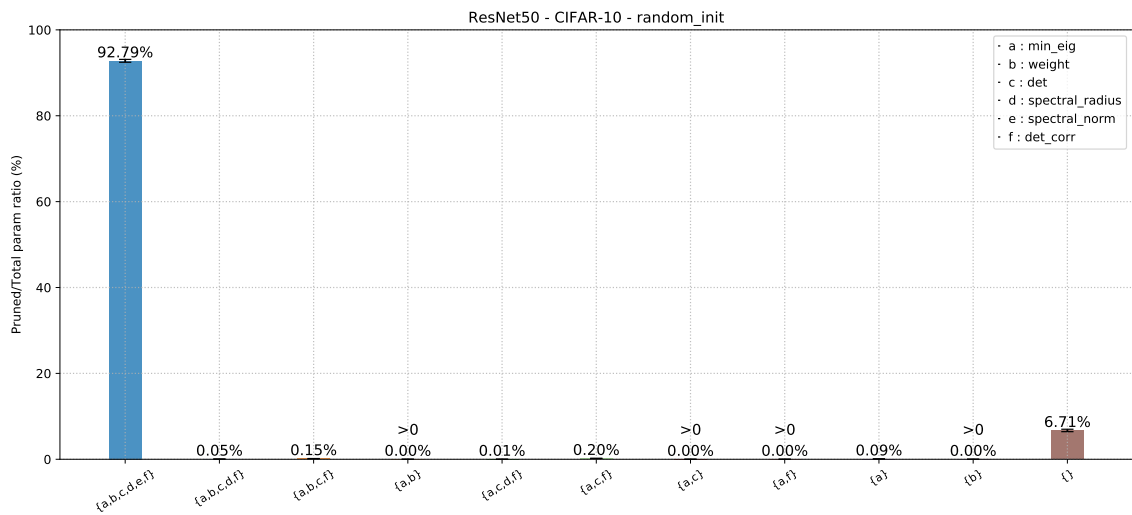


Figure 36: Set analysis bar chart for ResNet50 on CIFAR-100 with static\_init

## A Deeper Look into Convolutions via Pruning



**Figure 37:** Set analysis bar chart for ResNet50 on tiny-imagenet with static\_init



**Figure 38:** Set analysis bar chart for ResNet50 on CIFAR-10 with random\_init

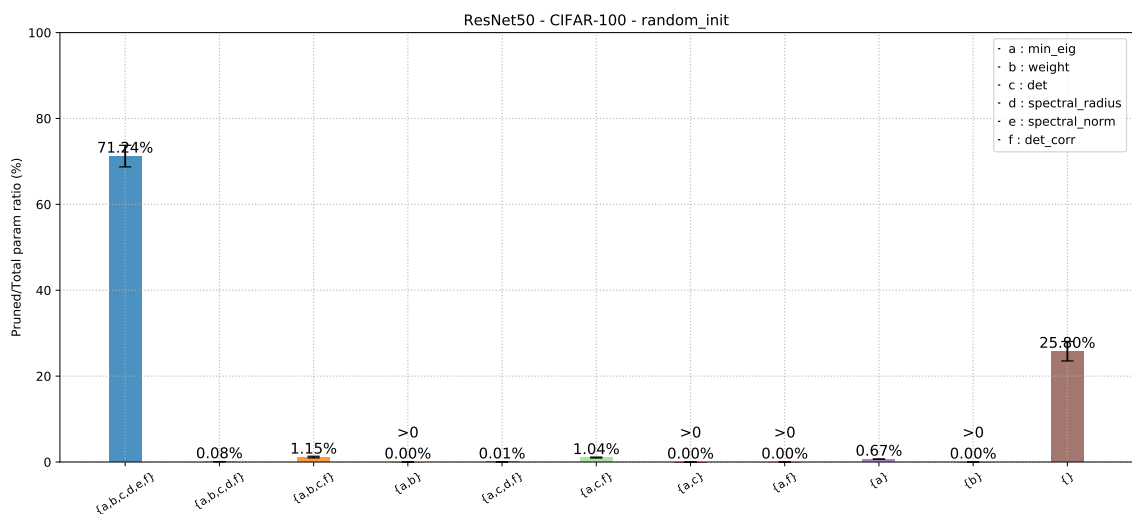


**Figure 39:** Set analysis bar chart for ResNet50 on CIFAR-100 with random\_init

## A Deeper Look into Convolutions via Pruning

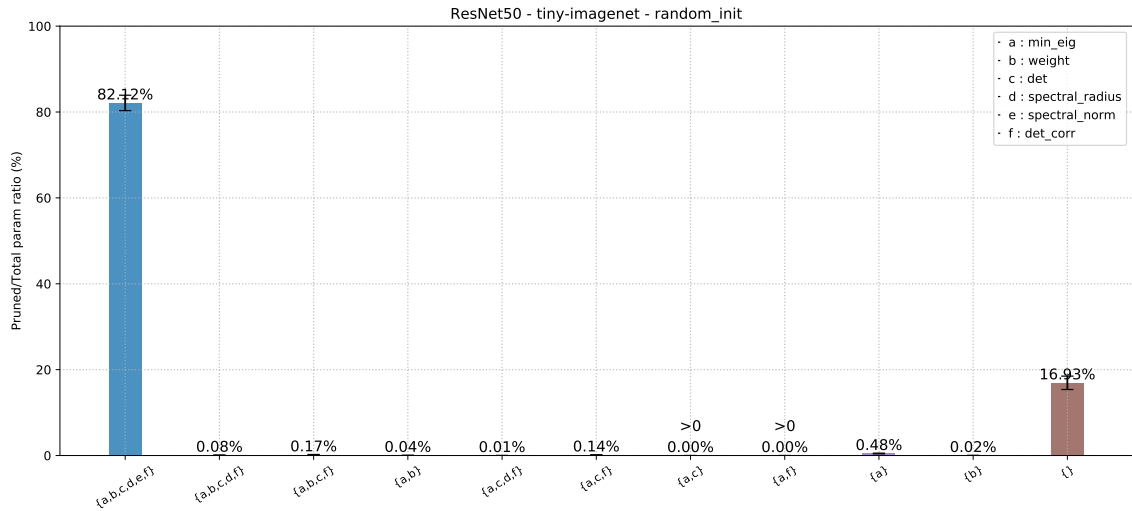


**Figure 40:** Set analysis bar chart for ResNet50 on tiny-imagenet with random\_init

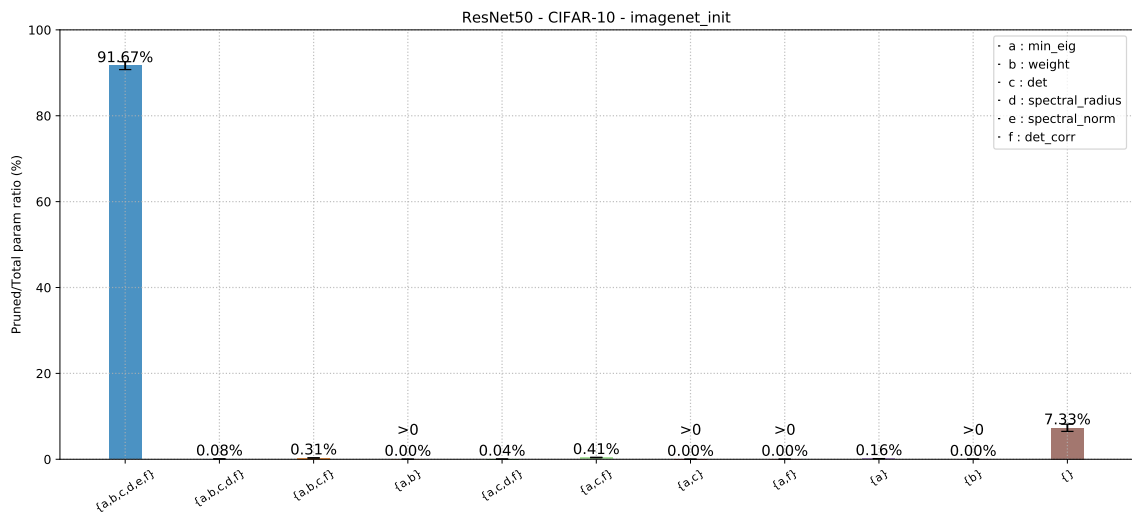


**Figure 41:** Set analysis bar chart for ResNet50 on CIFAR-10 with imagenet\_init

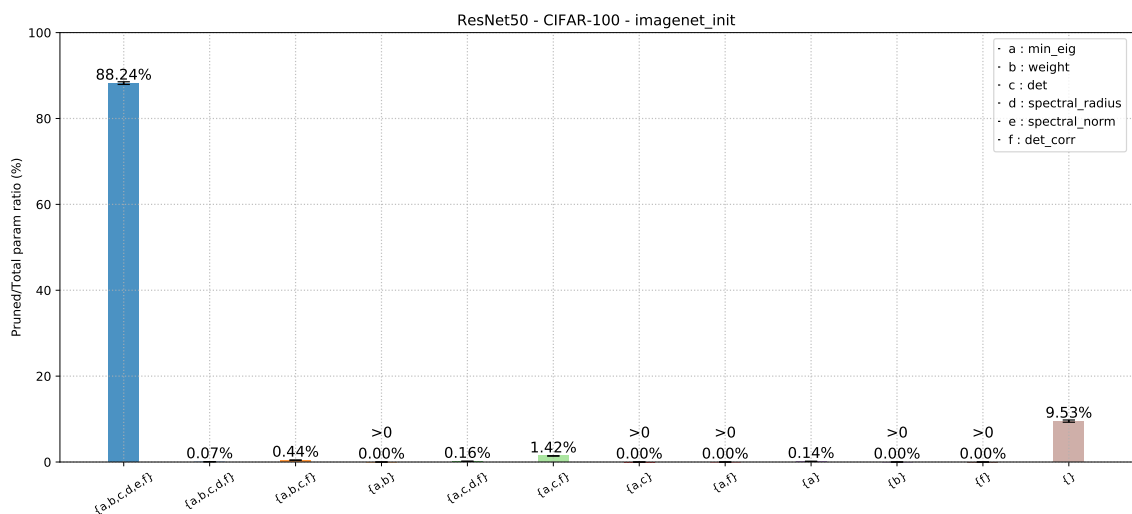


**Figure 42:** Set analysis bar chart for ResNet50 on CIFAR-100 with imagenet\_init

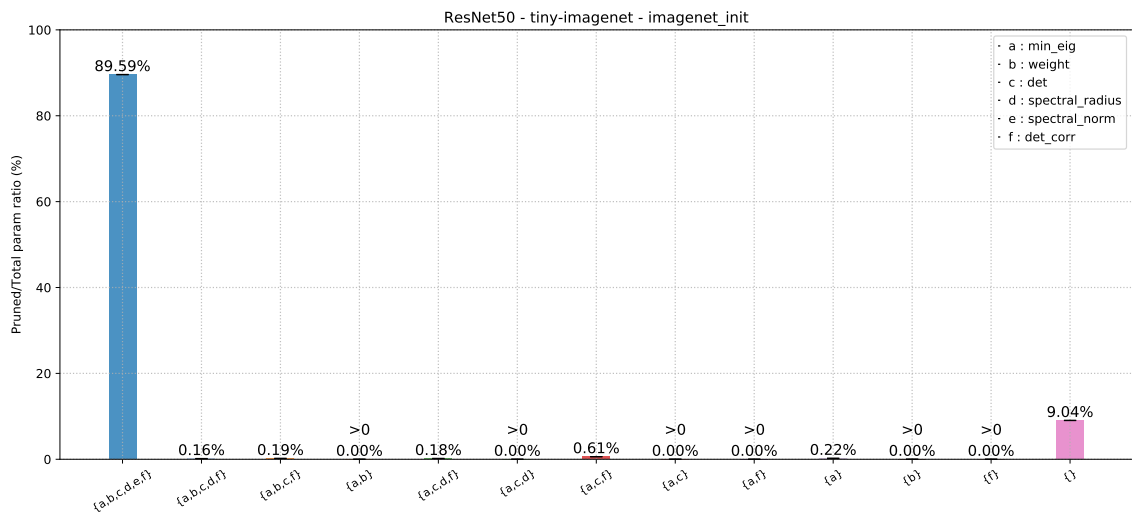


Figure 43: Set analysis bar chart for ResNet50 on tiny-imagenet with imagenet\_init